Effect of stress-induced magnetization on crack monitoring by self magnetic flux leakage method

Master thesis

S.L. van Kreveld

MSc Offshore & Dredging Engineering

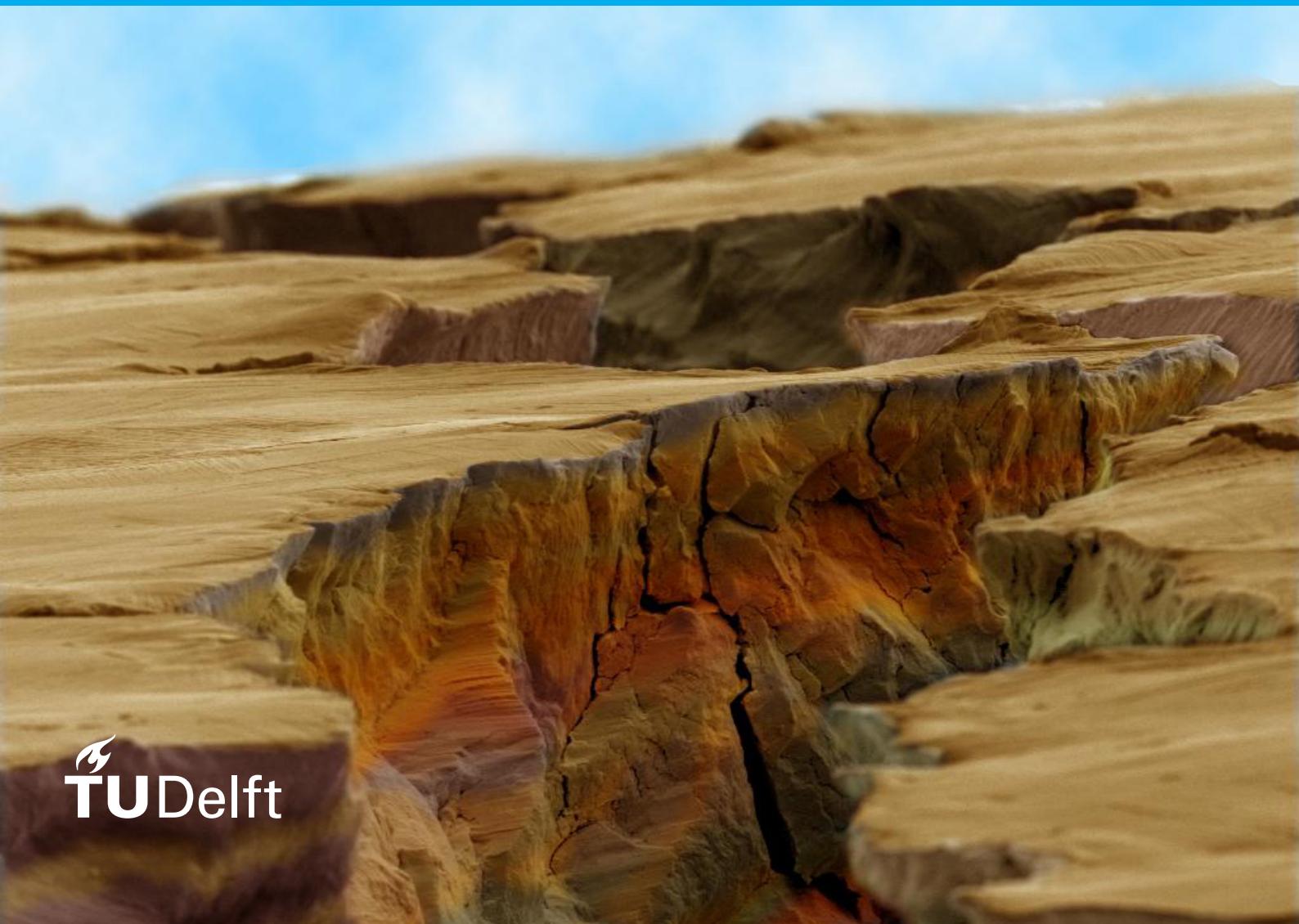

TU Delft

Effect of stress-induced magnetization on crack monitoring by self magnetic flux leakage method

by

S.L. van Kreveld

to obtain the degree of Master of Science
at the Delft University of Technology,
to be defended publicly on Thursday April 5, 2018 at 04:00 PM.

Student number:	4088581	
Project duration:	May 1st, 2017 – April 5th, 2018	
Thesis committee:	Prof. Dr. Ir. M. L. Kaminski,	TU Delft
	Ir. M. P. van der Horst,	TU Delft, supervisor
	Dr. Ir. M. Janssen,	TU Delft

TU Delft

TU Delft Delft University of Technology

Offshore & Dredging Engineering

Effect of stress-induced magnetization on crack monitoring by self magnetic flux leakage method

Fatigue cracks could occur in the material of offshore and marine structures that are cyclically loaded. These cracks occur due to the cyclic stresses induced by the waves causing premature failure. Monitoring these fatigue cracks using a wireless system gives the opportunity to guarantee the integrity of the structure without manual inspection, making this a safer way of inspection. In addition, inspection is very costly due to the man hours and because of the fact that the locations of fatigue cracks are mostly not easily accessible. Also, visual evaluation of the crack length can be difficult to assess, which could result in early retirement of structures or unnecessary and costly maintenance.

A wireless crack monitoring system based on the Self Magnetic Flux Leakage (SMFL) method could be a solution for this problem. This method suggests that the ferromagnetic material is passively magnetized by the Earth's magnetic field and the magnetic signal changes when a crack appears in the material. The measured data is sent wirelessly to the control room of the marine structure. Here, the data can be assessed to determine the size of the fatigue crack (figure 1). With this information, it can be decided what course of action should be taken to ensure the integrity of the marine structure as long as possible. This will result in a safer way of working and being economically more efficient.

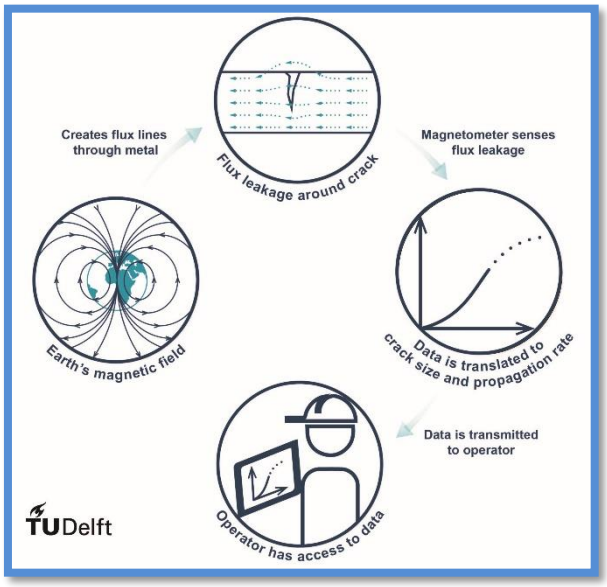

Figure 1 - Self magnetic flux leakage method

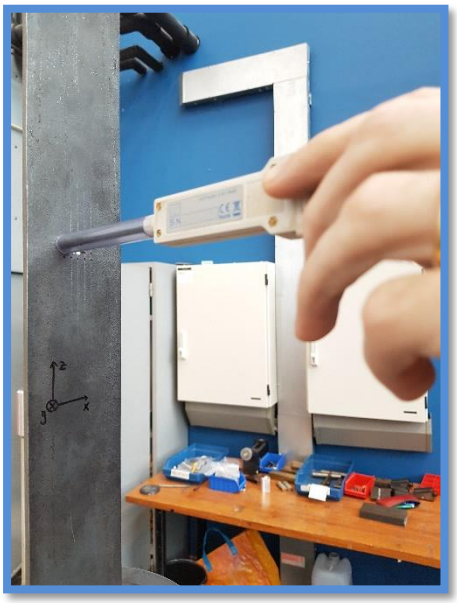

Figure 2 – Experimental setup

For accurate crack sizing, the SMFL must be interpreted correctly. During cyclic loading the stresses in the material change, affecting the magnetic signal. This is called the stress-induced magnetization. The aim of this research is to investigate the effect of stress-induced magnetization on the SMFL in the stress concentration zone of a structural steel plate, and its implications for crack monitoring by the SMFL method.

The measured stress magnetization curves are obtained by means of an experiment. In this experiment, a steel plate with an elliptical hole is cyclically loaded up to the yield stress. The magnetic signal is measured in a grid around the hole (figure 2). The results show a maximum variation of 25 µT. Depending on the application, the stress-induced magnetization may need to be considered for the interpretation of the measured signals for crack monitoring using the SMFL method.

Student
Sylvia van Kreveld
April 5th, 2018

Thesis committee
Prof. dr. ir. M.L. Kaminski
Ir. M.P. van der Horst
Dr. ir. M. Janssen

Contents

Nomenclature

Abbreviations

FEM	Finite Element Method
MMM	Magnetic Memory Method
SMFL	Self Magnetic Flux Density

List of Symbols - Magnetism		**Described on**
α	Interdomain coupling parameter	Page 7
δ	Directional parameter	
ϵ	Rate of approach parameter	
η	Reversibility coefficient for the magnetization due to stress	
λ	Magnetostriction	Page 6
μ_0	Permeability of free space	
μ_r	Relative permeability	Page 5
σ	Stress	
θ	Angle between the axis of applied stress and the magnetic field	
υ	Poisson's ratio	
ζ	Relation coefficient	Page 7
a	Form factor for the anhysteretic curve	
B	Magnetic flux density	Page 4
B_σ	Stress-induced magnetization	Page 6
B_{ind}	Induced magnetism	Page 6
B_{per}	Permanent magnetism	Page 6
c	Reversible wall motion component	
E	Young's modulus	
H	Magnetic field strength	Page 4
H_σ	Effective field caused by stress	Page 6
H_e	Total effective field	Page 6
k	Pinning constant	Page 7
k_b	Boltzmann's constant	
M	Magnetization	
m	Magnetical moment of a typical pseudomain	

M_a	Anhysteretic magnetization	Page 6
M_{irr}	Irreversible component of the magnetization	
M_s	Saturation magnetization	
T	Temperature	

List of Symbols - Fatigue		**Described on**
ΔK	Stress intensity factor range	Page 12
θ	Angle to determine location on the ellipse	Page 14
a	Crack length	
C	Material parameter	
M	Bulging correction factor	Page 13
M	Finite width correction factor	Page 13
m	Material parameter	
M_m	Geometry and crack size correction factor	Page 13
N	Cycles	
Y	Correction factor	Page 13

1 Introduction

1.1. General

Fatigue cracks could occur in the material of offshore and marine structures that are cyclically loaded. For example in the plate material of a ship, mooring lines, but also in bridges and all other steel structures that are cyclic loaded. These cracks occur due to the cyclic stresses induced by the waves causing premature failure. Monitoring these fatigue cracks using a wireless system gives the opportunity to guarantee the integrity of the structure without manual inspection of the structure, making this a safer way of inspection. In addition, inspection is very costly due to the man hours and because of the fact that the locations of fatigue cracks are mostly not easily accessible. Also, visual evaluation of the crack length can be difficult to assess, which could result in early retirement of structures or unnecessary and costly maintenance.

A wireless crack monitoring system based on the Self Magnetic Flux Leakage (SMFL) method could be a solution for this problem. This method suggests that the magnetic signal changes when a crack appears in the material. The measured data is sent wirelessly to the control room of the marine structure. Here, the data can be assessed to determine the size of the fatigue crack. With this information, it can be decided what course of action should be taken to ensure the integrity of the marine structure as long as possible. This will result in a safer way of working and being economically more efficient as in figure 1.1 is visualized.

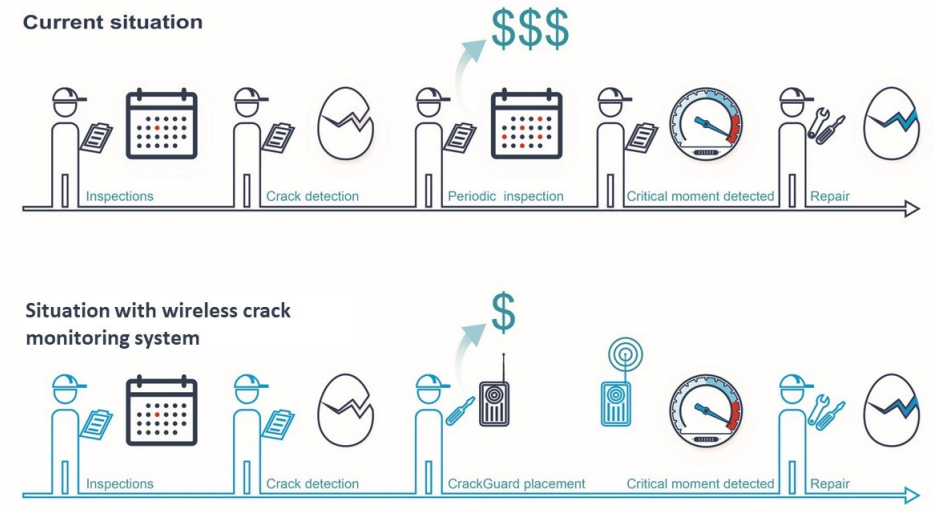

Figure 1.1: The benefits of using a wireless crack monitoring system

1.2. Problem Statement

The SMFL method is based on measurements with a Hall sensor. This sensor measures the amount of magnetic flux density in a particular direction. This unit is expressed in the dimension micro Tesla [μT]. Measur-

ing a change in magnetic flux density could give an indication for the crack length. This change can be caused by the occurrence of a crack or by other factors, like the magnetization induced by stresses in the material. For the data to be correctly assessed all the factors influencing the SMFL need to be researched. This thesis will focus on the changes in SMFL caused by stresses induced in the material.

1.3. Research objective

The main research question is:

- What effect does the stress-induced magnetization have on crack monitoring by self magnetic flux leakage on a steel plate?

The sub question that needs to be answered is the following:

- Is it possible to detect a fatigue crack in a steel plate that is in tension with a Hall sensor measuring the magnetic flux density?
- Does the magnetic flux density signal for a fatigue crack brought into tension behave the same as for cracks that are not?
- Is the effect of the stress-induced magnetization significant on the magnetic flux density signal of a steel plate with a fatigue crack?
- Does the effect of the stress-induced magnetization on the magnetic flux density signal of a steel plate with a crack correspond to the behavior described in the literature?
- What is the difference between the magnetic flux density signal of a plastically deformed part of the steel plate and the elastically deformed part?

These question will be answered in chapter 6 and discussion and recommendations for these results can be found in chapter 7.

2

Theory and literature study

2.1. Introdution

In this section the measuring technique for the self magnetic flux leakage method is explained. This method can be influenced by several effects. Two of these effects are the crack opening effect and the stress-induced magnetization. These effects will be discussed in more detail. This chapter ends with the explanation about the three stages of fatigue.

2.2. Magnetic Testing

2.2.1. Introduction

The self magnetic flux leakage method is a non destructive evaluation method for monitoring fatigue cracks. This method is based on measuring the magnetic signal which means that the steel structure needs to be magnetized. The steel material is not actively magnetized by other magnets or coils for this method. The structure is solely magnetized by the Earth's magnetic field which is called passive magnetization. This creates flux lines through the metal. When a crack appears these flux lines 'leak' out of the metal into the air. This is explained in more detail in this section. The leaking flux can be measured with a magnetometer which measures the magnetic signal. This data can be translated to a crack length with appropriate knowledge of this signal. This knowledge is extended with the effect of the induced stresses on the magnetic signal. The data is send wireless to the operator and he can assess what course of action needs to be taken to maintain the integrity of the structure. This is schematically illustrated in figure 2.1.

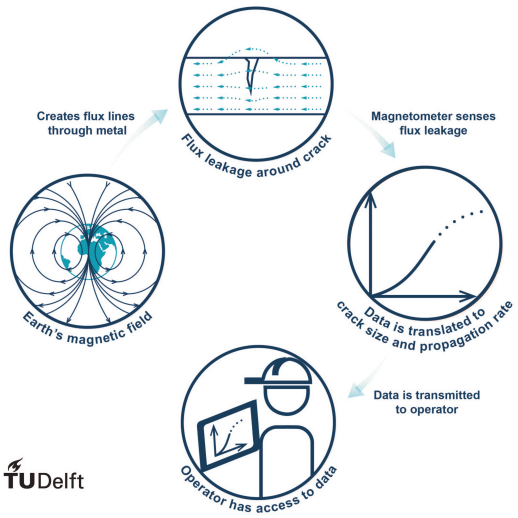

Figure 2.1: Schematic explanation SMFL method

2.2.2. Ferromagnetic materials

Materials that can be magnetized are called ferromagnetic materials. They have magnetic domains due to their crystalline structure. Each of these domains has a remanent magnetization, which is the 'spontaneous magnetization' without an external magnetic field being applied. If an external magnetic field is applied the magnetic domains are aligned resulting the material being magnetized [7]. This is schematically illustrated in figure 2.2 in reality the shape and location of the domains change as well but this is not illustrated.

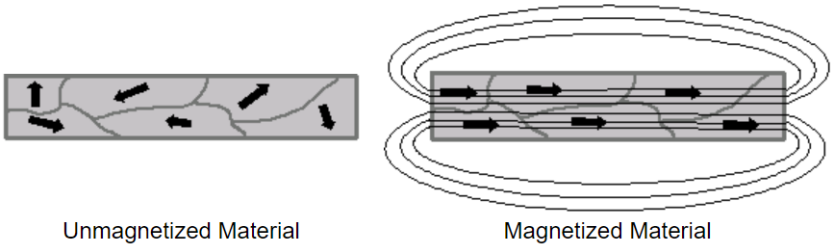

Figure 2.2: Magnetic domains aligned for magnetization [7]

These domains act as dipoles. The walls of the domains are pinned and experience domain wall bulging and displacement. Domain wall bulging is reversible but domain wall displacement is irreversible, which is illustrated in figure 2.3. This makes that ferromagnetic materials show hysteretic behavior between the magnetic flux density (B) in the material and the magnetic field strength (H). The magnetic flux density B can be best explained as a measure of the actual magnetic field within a material. This can be expressed as the concentration of magnetic flux per unit cross-sectional area and is measured in micro Tesla [μT]. The magnetic field strength H is a measure of the magnetizing field produced by the Earth's magnetic field and surroundings. This is measured in ampere per meter [A/m] [6]. A schematic drawing of the hysteresis curve is presented in figure 2.4.

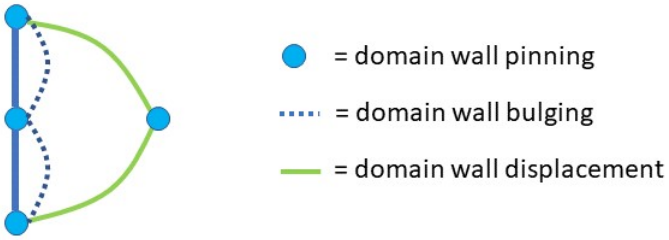

Figure 2.3: Domain wall pinning, bulging and displacement

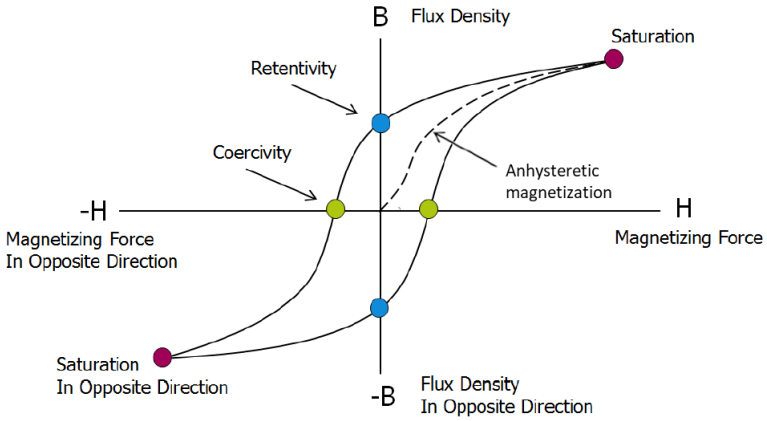

Figure 2.4: Hysteresis curve [28]

2.2.3. Self Magnetic Flux Leakage Testing

As explained in 2.2.1 the self magnetic flux leakage method is used for testing. This method makes use of the metal magnetic memory method (MMM). This is based on the fact that ferromagnetic materials can be passively magnetized by its surroundings and the Earth's magnetic field [17]. This field has an intensity H of 49 A/m in Delft (Netherlands) according to the World Magnetic Model 2014 - 2019. For steel this is a very small magnetizing force. Still, this enough to magnetize the material causing the magnetic flux density to increase in the steel structure.

In this section two phenomenon are explained that can influence the measured magnetic flux density: the opening of the crack and the stress in a material, called the magnetomechanical effect.

Crack opening effect

The magnetic flux lines in magnetized material will always take the path of the least resistance. This depends on the magnetic permeability, which is the relative increase or decrease in the resultant magnetic field inside the material in comparison to the magnetizing field where the given material is located [6].

The SMFL method shows that in the vicinity of a crack there is a sudden decrease of magnetic permeability due to the crack opening. This is caused by the low relative permeability of air $\mu_r = 1.0$ [15] in comparison to ±225 [27] for a structural steel plate. This relative small difference causes some magnetic flux to 'leak' out of the material into the air and returns into the steel at the other side of the crack [28].

The flux lines that leaked into the air can be measured with a magnetometer (Hall sensor) as shown in figure 2.5. Figure 2.6 shows the flux leakage signal presented by the blue line. The search coil of the magnetometer gives an output presented by the red line. This results in a positive and negative half-peak in the output of the magnetometer, when crossing the crack as can be seen in figure 2.6. This can be explained by local North and South pole that will occur on both sides of the crack [27]. Near the crack tip the flux lines will remain in the material and go around the crack which causes a concentration of flux lines at the crack tip.

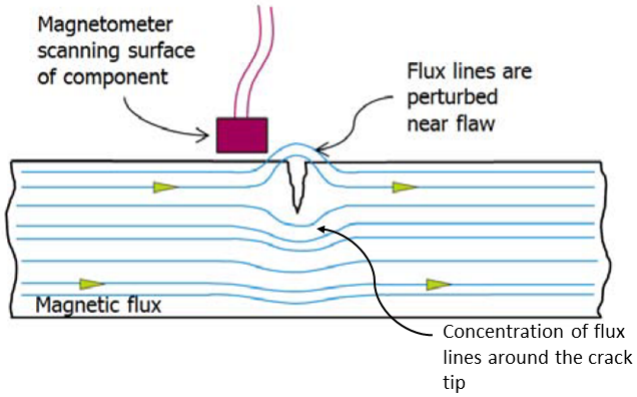

Figure 2.5: Magnetic leakage flux measurement with magnetometer

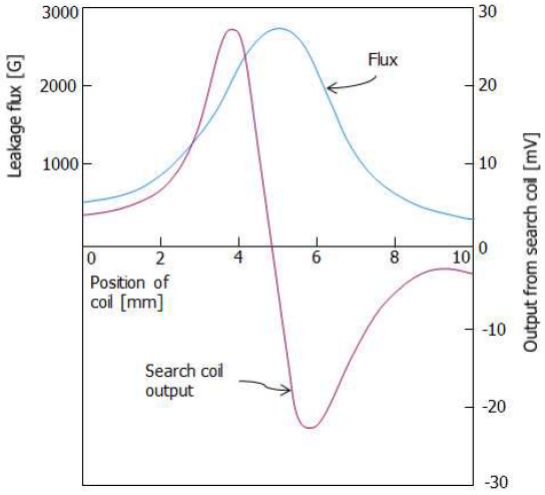

Figure 2.6: Variation of leakage flux with distance across a crack [11]

This signal is caused by two factors: the induced magnetism and the permanent magnetism of the material. The induced magnetism is the magnetic field caused by the surroundings of the material including the Earth's magnetic field. For small fields it can be assumed that this hysteretic curve behaves linear [26]. The induced magnetization is proportional with the applied field and changes instantaneously. The permanent magnetism is due to the ferromagnetic properties of the material and behaves therefore hysteretic. Also, the permanent magnetism is not homogeneously distributed in the material. This field can be determined according to Van der Horst [27].

$$B = B_{ind} + B_{per} \tag{2.1}$$

Magnetomechnical Effect

A part of the permanent magnetism in equation 2.1 is due to the magnetization caused by stresses induced in the material, this phenomenon is called the magnetomechanical effect and is explained in this section. This phenomenon is part of the permanent magnetism and therefore it will also behave hysteretic. In this research the assumptions is made that the stress-induced magnetization can be separated from the permanent magnetism as follows.

$$B = B_{ind} + B_{per} + B_{\sigma} \tag{2.2}$$

The magnetomechanical effect is the effect that stress has on the magnetization of a material. According to [18] the magnetization caused by this phenomenon can be modeled according the equations 2.3 to 2.7.

The effect of stress on the magnetization can be approximated as an effective field described by equation 2.3. In this equation the magnetostriction is denoted by λ. This is the change in dimension of a piece of magnetic material induced by a change in its magnetic state [16], which can also be explained as the strain caused by the magnetic field. With the effective field description (equation 2.3) the total effective field can be calculated including the stress contribution as shown in equation 2.4.

It is assumed that the stress dependence of the anhysteretic magnetization can be based on the generalized Langevin function shown in equation 2.5. The anhysteretic magnetization is the change in magnetization without hysteretic effects, also described as the energy present prior to when domain wall bulging occurs. This is indicated in the hysteresis curve in figure 2.4. Equation 2.5 depends on the material that is chosen and in this model isotropic materials are assumed. The final differential equation for the irreversible, reversible and anhysteretic components for the magnetization is given by equation 2.7.

$$H_{\sigma} = \frac{3}{2}\frac{\sigma}{\mu_0}\frac{d\lambda}{dM}(cos^2\theta - vsin^2\theta) \tag{2.3}$$

$$H_e = H + \alpha M + H_\sigma \tag{2.4}$$

$$M_a = M_s\Big[coth\Big(\frac{H_e}{a}\Big) - \frac{a}{H_e}\Big] \tag{2.5}$$

where

$$a = \frac{k_b T}{\mu_0 m} \tag{2.6}$$

$$\frac{dM}{d\sigma} = \frac{1}{\epsilon^2}(\sigma \pm \eta E)(1-c)(M_a - M_{irr}) + c\frac{dM_a}{d\sigma} \tag{2.7}$$

where

$$\epsilon = (E \cdot \zeta)^{0.5} \tag{2.8}$$

Parameter	**Unit**	**Represents**
σ	[Pa]	Stress
λ	[-]	Magnetostriction
M	[A/m]	Magnetization
μ_0	$[\frac{mkg}{s^2A^2}]$	Permeability of free space
θ	[rad]	Angle between the axis of the applied stress and the axis of the magnetic field
υ	[-]	Poisson's ratio
α	[-]	Dimensionless mean field parameter representing interdomain coupling
M_s	[A/m]	Saturation magnetization
k_b	$[\frac{m^2kg}{s^2K}]$	Boltzmann's constant
T	[K]	Temperature
m	[J/T]	Magnetic moment of a typical pseudomain
E	[Pa]	Young's modulus
M_{irr}	[A/m]	The irreversible component of magnetization
c	[-]	Reversible wall motion component
ϵ	[Pa]	Rate of approach parameter
ζ	$[\frac{kg}{ms^2}]$	Coefficient relating the derivative of irreversible magnetization with respect to elastic energy to the displacement of the irreversible magnetization from the anhysteretic magnetization
η	[-]	Coefficient which represents reversible change in the magnetization with the action of stress

Table 2.1: Parameters for equations 2.3 to 2.7

This model theory is based on the concept, when a material is under changing applied stress and a constant magnetic field, the magnetization changes and will approach the anhysteretic magnetization [18]. Also, it takes into account the asymmetry in response to tension or compression. Experiments in mild steel [14] have shown that there is asymmetry under compression and in tension.

Effective field description

Since this thesis focuses on the change in magnetization due to the stress a relation needs to be derived for the magnetization depending on the stress. This can be done according to the effective field description [23] which is based on the description of the magnetomechanical effect [18] as described before. This derivation was done by PhD student Aad Vijn from the faculty of Applied Mathematics at the Delft University of Technology.

For this case a constant magnetic applied field H_a and a varying stress σ is assumed. This description of the effective field is done under the assumption that the magnetostriction is very small and the applied field has the same direction as the direction of the applied stress.

The effective field H_e is described in equation 2.9.

$$H_e = H_a + \alpha M + H_\sigma \tag{2.9}$$

where

$$H_\sigma = \frac{3}{2\mu_0}\sigma\frac{\partial\lambda}{\partial M} \tag{2.10}$$

The magnetostriction λ is expanded as a power serie.

$$\lambda(M,\sigma) = \sum_{i=0}^{\infty}\gamma_i(\sigma)M^{2i} \tag{2.11}$$

where

$$\gamma_i(\sigma) = \sum_{n=0}^{\infty}\frac{\sigma^n}{n!}\gamma_i^{(n)}(0) \tag{2.12}$$

The increment dH_e is

$$dH_e = \alpha dM + dH_\sigma \tag{2.13}$$

Due to the product rule dH_σ becomes

$$dH_\sigma = \frac{3}{2\mu_0}\Big(\sigma\frac{\partial^2\lambda}{\partial M^2}dM + \sigma\frac{\partial^2\lambda}{\partial M\partial\sigma}d\sigma + \frac{\partial\lambda}{\partial M}d\sigma\Big) \tag{2.14}$$

The notation according to [23] is followed.

$$A_1(M,\sigma) = \frac{\partial H_e}{\partial M} = \alpha + \frac{3\sigma}{2\mu_0}\frac{\partial^2\lambda}{\partial M^2} \tag{2.15}$$

$$A_2(M,\sigma) = \frac{3}{2\mu_0}\Big(\frac{\partial\lambda}{\partial M} + \sigma\frac{\partial^2\lambda}{\partial M\partial\sigma}\Big) \tag{2.16}$$

The following differential equation for the effective field is proposed

$$(M - M_a) = -k\delta\frac{dM}{dH_e}, \tag{2.17}$$

where M_a is the anhysteretic magnetization, k is the pinning constant and δ is the directional parameter, which is either positive or negative for increasing or decreasing fields.

The anhysteretic magnetization is given by

$$M_a(H_e) = M_s\mathscr{L}(H_e/a) \tag{2.18}$$

where M_s is the saturation magnetization, a being a hysteresis parameter and $\mathscr{L}$ is the Langevin function presented in equation 2.19.

$$\mathscr{L}(x) = coth(x) - 1/x \tag{2.19}$$

So, under a constant field the differential equation may be written as

$$dH_e = A_1(M,\sigma)dM + A_2(M,\sigma)d\sigma \tag{2.20}$$

when multiplied with $(M - M_a)$ this results in

$$(M - M_a)dH_e = A_1(M - M_a)dM + A_2(M - M_a)d\sigma \tag{2.21}$$

This can be simplified with equation 2.17 into

$$-k\delta dM = A_1(M - M_a)dM + A_2(M - M_a)d\sigma \tag{2.22}$$

Hence,

$$\{k\delta + A_1(M - M_a)\}dM + A_2(M - M_a)d\sigma = 0 \tag{2.23}$$

is the differential obtained that describes the connection between the varying stress and the magnetization and this can be written as the following differential equation.

$$\frac{dM}{d\sigma} = -\frac{A_2(M,\sigma)(M - M_a)}{k\delta + A_1(M,\sigma)(M - M_a)} \tag{2.24}$$

This differential equation is extended by Naus [23] to include the reversible contribution of the magnetization. This equation is extended with constant c which is the reversible wall motion component.

$$\frac{dM}{d\sigma} = -\frac{A_2(M,\sigma)(M - M_a - ck\delta\frac{dM_a}{dH_e})}{k\delta + A_1(M,\sigma)(M - M_a - ck\delta\frac{dM_a}{dH_e})} \tag{2.25}$$

This can be solved numerically with the Euler forward method. For this it is needed to tale the first two terms in the expansion for $\lambda(M,\sigma)$

$$\lambda = \gamma_0(\sigma) + \gamma_1(\sigma)M^2 \tag{2.26}$$

where

$$\gamma_0(\sigma) = \gamma_0^0 + \gamma_0^1\sigma \tag{2.27}$$

$$\gamma_1(\sigma) = \gamma_1^0 + \gamma_1^1\sigma \tag{2.28}$$

and $\gamma_0^0, \gamma_0^1, \gamma_1^0, \gamma_1^1 \in \mathbb{R}$

The partial derivatives reads

$$\frac{\partial\lambda}{\partial M} = 2\gamma_1(\sigma)M \tag{2.29}$$

$$\frac{\partial^2\lambda}{\partial M^2} = 2\gamma_1(\sigma) \tag{2.30}$$

$$\frac{\partial^2\lambda}{\partial\sigma\partial M} = \frac{\partial}{\partial\sigma}\Big(\frac{\partial\lambda}{\partial M}\Big) = \frac{\partial}{\partial\sigma}(2\gamma_1(\sigma)M) \tag{2.31}$$

So, in fact, all derivations of interest are expressed in terms of $\gamma_1(\sigma)$, that is in terms of γ_1^0 and γ_1^1.
In what follows it is written

$$\gamma_1(\sigma) = \eta + \omega\sigma \tag{2.32}$$

,so $\eta \equiv \gamma_1^0$ and $\omega \equiv \gamma_1^1$
This results in the partial derivatives to be denoted as follows.

$$\frac{\partial\lambda}{\partial M} = 2M(\eta + \omega\sigma) \tag{2.33}$$

$$\frac{\partial^2 \lambda}{\partial M^2} = 2(\eta + \omega\sigma) \tag{2.34}$$

$$\frac{\partial^2 \lambda}{\partial \sigma \partial M} = 2\omega M \tag{2.35}$$

The auxiliary functions A_1 and A_2 now reads

$$A_1(M,\sigma) = \alpha + \frac{3\sigma}{2\mu_0}(2\eta + \omega\sigma) = \alpha + \frac{3\eta}{\mu_0}\sigma + \frac{3\omega}{2\mu_0}\sigma^2 \tag{2.36}$$

$$A_2(M,\sigma) = \frac{3\sigma}{2\mu_0}(2M(\eta + \omega\sigma) + \sigma 2\omega M) = \frac{3\eta}{\mu_0}M + \frac{6\omega}{\mu_0}M\sigma \tag{2.37}$$

This results in that the differential equation may be written as:

$$-\frac{dM}{d\sigma} = \frac{(M - M_a - ck\delta\frac{dM_a}{dH_e})\left(\frac{3\eta}{\mu_0}M + \frac{6\omega}{\mu_0}M\sigma\right)}{k\delta + (M - M_a - ck\delta\frac{dM_a}{dH_e})\left(\alpha + \frac{3\eta}{\mu_0}\sigma + \frac{3\omega}{2mu_0}\sigma^2\right)} \tag{2.38}$$

By introducing the following denotations the differential equation can be written as equation 2.41.

$$B_1 \equiv \frac{3\eta}{\mu_0} \quad \in \mathbb{R} \tag{2.39}$$

$$B_2 \equiv \frac{6\omega}{\mu_0} \quad \in \mathbb{R} \tag{2.40}$$

$$\frac{dM}{d\sigma} = -\frac{(M - M_a - ck\delta\frac{dM_a}{dH_e})(B_1 M + B_2 M\sigma)}{k\delta + (M - M_a - ck\delta\frac{dM_a}{dH_e})(\alpha + B_1\sigma + \frac{1}{4}B_2\sigma^2)} \tag{2.41}$$

where

$$M_a = M_a(H_e) = M_a(H_a + \alpha M + H_\sigma) \tag{2.42}$$

$$H_\sigma = \frac{3}{2\mu_0}\sigma\frac{\partial\lambda}{\partial M} = B_1 M + 2B_2 M\sigma \tag{2.43}$$

The values used for $\eta = 3\cdot 10^{-18}$ and for $\omega = 0$ according to Naus [23].

To solve this differential equation 5 hysteresis parameters are needed to describe this model. These parameters are determined according to Jiles [19]. In which the parameters are calculated with an algorithm by using the measured properties at the origin, loop tip, remanence and coercivity. This gave an approximation of the curve after which the parameters were manually optimized to obtain the best fit for the entire measured curve. In the experiments described in this thesis, steel with a yield strength of 235 MPa is used which has a maximum carbon content of 0.22 wt% [2]. For that reason, the model parameters for Fe 0.2 wt% C [2] were used.

Parameter	Unit	Represents
M_s	$1.6\cdot 10^6$ [A/m]	Saturation magnetization
a	1085 [A/m]	Form factor for the anhysteretic curve
k	320 [A/m]	Pinning constant, parameter that determines the hysteresis loss
α	$2\cdot 10^{-3}$ [-]	Interdomain coupling parameter
c	0.3[-]	Reversible wall motion component

Table 2.2: Model hysteresis parameters for Fe 0.2 wt% C [19]

The effective field description can numerically be solved with the Euler forward method. This method solves the ordinary differential equation by

$$y_{n+1} = y_n + hf(x_n, y_n) \tag{2.44}$$

the solution advances from x_n to $x_{n+1} = x_n + h$ [4]. For this method it is important to ensure stability according to the Courant-Friedrichs-Lewy condition. This conditions states that the time step should be chosen that is smaller than a certain time used in many explicit computer simulations [1]. In the model of the effective field description the stability is ensured by applying a sufficient large initial field.

2.3. Fatigue Cracks

2.3.1. Forming of fatigue cracks

There are three stages in forming of fatigue cracks [10]:

- crack initiation
- slow crack propagation
- sudden propagation leading to fracture

When crack initiation and slow crack propagation occurs, the structural integrity is still maintained until the critical crack length, till this point the residual strength in the material is still within the design strength of the structure [21]. This is illustrated in figure 2.7. Due to the uncertainty of the crack growth, the structure needs to be inspected more frequently when there is a significant crack or even taken out of service for maintenance earlier than necessary. Estimating this point more precisely can lead to saving on maintenance costs since no man hours are needed and the frequency can be lowered of taking the structure out of service for maintenance [27].

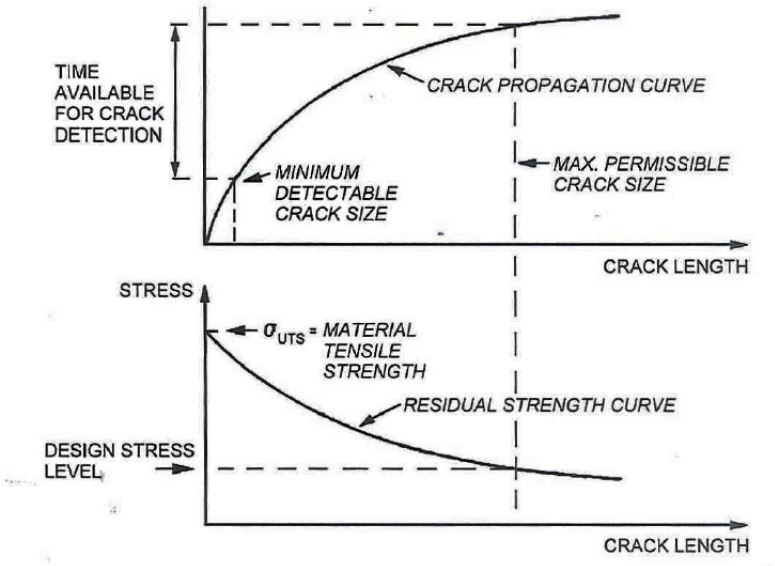

Figure 2.7: Maximum permissible crack length for design stress level [21]

Crack Initiation

Waves and other vibrations cause cyclic loading in marine and offshore structures. These vibrations can initiate micro fractures in the material of steel structures.

These micro fractures occur under cyclic loading due to the accumulation of dislocations in the material resulting in persistent slip bands (PSB) shown in figure 2.8. Along the slip plane of the material these PSB's

will cause intrusions and extrusions resulting in a stress concentration which can lead to fatigue cracks under continues cyclic loading [8].

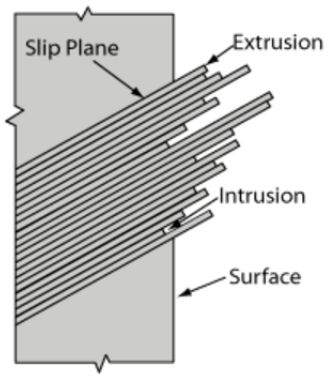

Figure 2.8: Persistent slip bands [8]

For fatigue cracks to initiate the fatigue threshold, ΔK_{th}, needs to be reached or exceeded. This is a function of a number of variables, including the material, the test conditions, the R-ratio, and the environment [22]. These values are presented in the ASM handbook [22] for different materials. In this thesis mild steel is used which has a threshold of 6.4 MPa$\sqrt{m}$ for a stress ration of R = 0.16.

Slow Crack Propagation

After initiation the fatigue crack keeps propagating under cyclic loading. The crack will propagate up to a certain crack length 'a' for every cycle 'N'. The relation for the crack propagation rate is the Paris's law in equation 2.45.

$$\frac{da}{dN} = C(\Delta K)^m \tag{2.45}$$

In this equation $\frac{da}{dN}$ is the crack growth rate per cycle, $\Delta K = K_{max} - K_{min} = (\sigma_{max} - \sigma_{min})\sqrt{\pi a}$ is the stress intensity factor range and C & m depend on the material, environment, frequency, temperature and stress ratio [25].

When the fatigue crack has not reached its critical length, the integrity of the structure is still retained. Wirelessly monitoring the fatigue crack using SMFL method in this stage could be an improvement. Since the course of action can be assessed before final fracture, without expensive human inspection or premature maintenance.

Sudden Propagation Leading to Fracture

When the critical crack length is reached sudden propagation of the fatigue crack will occur. This will result in fracture of the material. This should be avoided at all times since this would cause failure of the structure. If the fatigue cracked is monitored using SMFL method then maintenance can be performed on time. Resulting in maintaining the structural integrity of the structure.

In figure 2.9 the three stages of crack growth are presented and the area where the Paris' law is applicable.

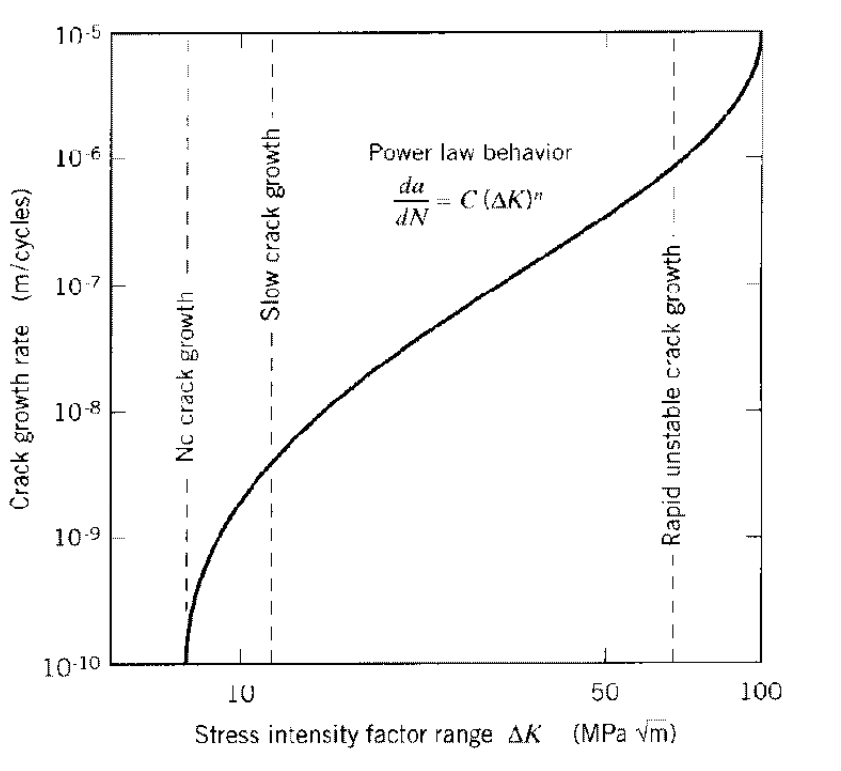

Figure 2.9: Three stages of crack growth [25]

2.3.2. Semi-Elliptical surface fatigue cracks

For semi-elliptical fatigue cracks in axial tension there are two directions of propagation possible both are perpendicular to the loading direction. The crack can propagate in sideways x-direction (also referred to as in the direction of c) or in the z-direction which is in the depth of the specimen (also referred to as in the direction of a) indicated in figure 2.11. This results in that everywhere along the ellipse there is a different stress intensity factor and these values differ depending on the geometry. Meaning it can either initiate in the direction of c (indicated by * in figure 2.11) or in the direction of a (indicated by · in figure 2.11).

The delta stress intensity factor along every point of the ellipse is given by the following equations given by the British Standard [12]. Figure 2.10 indicates that θ is the parameter that determines the location at the ellipse for which the delta stress intensity factor is calculated. The parameter a is the depth of the ellipse, 2c the width of the ellipse, t the thickness of the plate.

$$\Delta K = \Delta\sigma Y\sqrt{\pi a} \tag{2.46}$$

with

$$Y = M \cdot f_w \cdot M_m \tag{2.47}$$

M is for the bulging correction factor and for surface cracks in this case $M = 1$. The correction for finite width is given by

$$f_w = \left(sec\left[\left(\frac{\pi c}{W}\right)\left(\frac{a}{t}\right)^{0.5}\right]\right)^{0.5} \tag{2.48}$$

M_m is a geometry and crack size correction factor given by the following equations.

$$M_m = \left[M_1 + M_2\left(\frac{a}{t}\right)^2 + M_3\left(\frac{a}{t}\right)^4\right] \cdot f_\theta \cdot g/\phi$$

$$M_1 = 1.13 + 0.09\left(\frac{a}{c}\right) \qquad \text{for } 0 < a/2c \leq 0.5$$

$$M_1 = \left(\frac{c}{a}\right)^{0.5}\left[1 + 0.04\left(\frac{c}{a}\right)\right] \quad \text{for } 0.5 < a/2c \leq 1.0$$

$$M_2 = -0.54 + \left[\frac{0.89}{0.2 + \frac{a}{c}}\right] \quad \text{for } 0 < a/2c \leq 0.5$$

$$M_2 = 0.2\left(\frac{c}{a}\right)^4 \quad \text{for } 0.5 < a/2c \leq 1.0$$

$$M_3 = 0.5 - \frac{1.0}{0.65 + \frac{a}{c}} + 14\left(1.0 - \frac{a}{c}\right)^{24} \quad \text{for } 0 < a/2c \leq 0.5$$

$$M_3 = -0.11\left(\frac{c}{a}\right)^4 \quad \text{for } 0.5 < a/2c \leq 1.0$$

$$\phi = 1 + 1.464\left(\frac{a}{c}\right)^{1.65}$$

$$g = 1 + \left[0.1 + 0.35\left(\frac{a}{t}\right)^2\right](1 - sin(\theta))^2 \quad \text{for } 0 < a/2c \leq 0.5$$

$$g = 1 + \left[0.1 + 0.35\left(\frac{c}{a}\right)\left(\frac{a}{t}\right)^2\right](1 - sin(\theta))^2 \quad \text{for } 0.5 < a/2c \leq 1.0$$

$$f_\theta = \left[\left(\frac{a}{c}\right)cos(\theta)^2 + sin(\theta)^2\right]^{\frac{1}{4}} \quad \text{for } 0 < a/2c \leq 0.5$$

$$f_\theta = \left[\left(\frac{a}{c}\right)cos(\theta)^2 + sin(\theta)^2\right]^{\frac{1}{4}} \quad \text{for } 0.5 < a/2c \leq 1.0$$

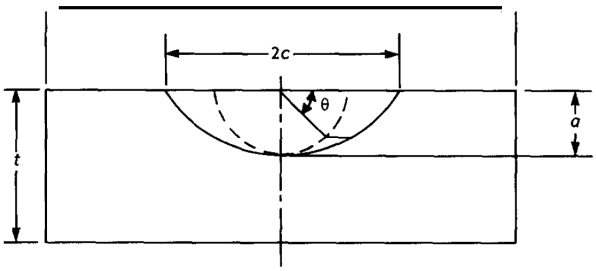

Figure 2.10: θ parameter determines location at the ellipse [20]

As explained before there are two directions in which the crack can start propagating. These points have a different stress intensity factors that can be used in Paris' law 2.45. This can be combined into one differential equation 2.49 to predict the shape changes of the ellipse after a certain amount of cycles [13].

$$\frac{da}{dc} = \left[\frac{\Delta K_a}{\Delta K_c}\right]^m = \left[\frac{M_a}{M_c}\right]^m \left[\frac{a}{c}\right]^{\frac{m}{2}} \tag{2.49}$$

where $K_{\{a,c\}} = M_{\{a,c\}}\sigma\sqrt{\pi\{a,c\}}$ with M_a and M_c being the stress intensity factor calibrations in the x-direction and y-direction.

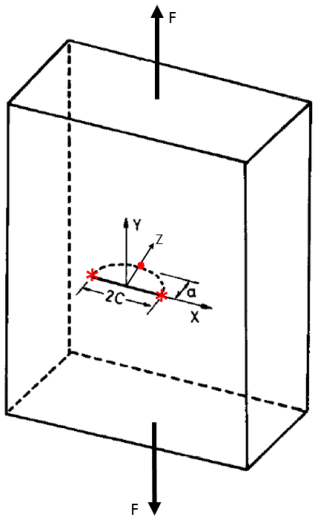

Figure 2.11: Semi-elliptical defect indicating points of crack initiation [13]

3

Experimental Testing

3.1. Introduction

To answer the research questions three experiments were conducted. In this chapter the experimental method is described for each of these experiments.

3.2. Experiment fatigue crack

3.2.1. Geometry

For the this experiment a plate with the dimensions presented in figure 3.1 is used. The dimensions of the defect in the plate are shown in figure 3.2. The plate has a thickness of 5 mm and is made out of steel with a yield strength of 235 MPa.

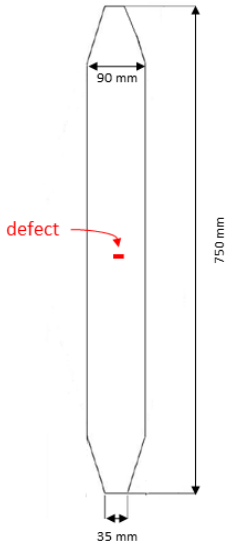

Figure 3.1: Geometry plate with semi-elliptical surface defect

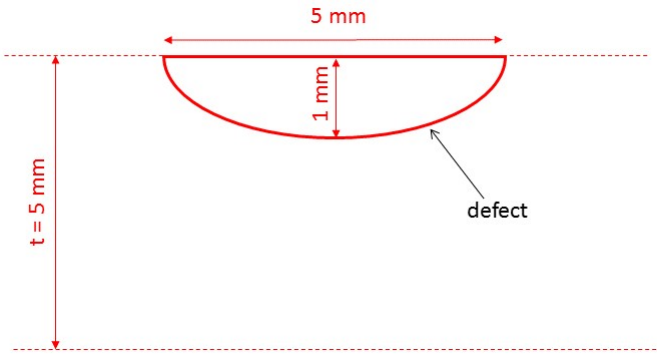

Figure 3.2: Semi-elliptical surface defect

3.2.2. Experimental setup

Figure 3.3 shows the experimental setup. The specimen is axially loaded in a MTS fatigue testing machine, that has a maximum range of -350 kN to 350 kN, to induce a fatigue crack in the specimen. For this experiment the magnetic flux density is measured with a Hall sensor with a sensitivity 1 μT [5] at the opposite side of the defect as shown in figure 3.3. The distance between the plate and the probe is kept constant at 1 mm. The magnetic flux density is measured in y direction (out of plane) for a grid of 40 mm in x direction and 20 mm z direction, with a spacing of 10 mm, positioned in the middle of the plate which is shown in figure 3.4. Also, this figure shows how the x, y and z axis are chosen. For every millimeter of crack propagation, the fatigue test is paused and a measurement has been performed. For every measurement the entire grid was measured twice, for a closed and for an open crack. The first measurement for a closed crack was done by approaching a force of zero on the specimen. The second measurement for an open crack was done by setting the maximum tensile load on the specimen.

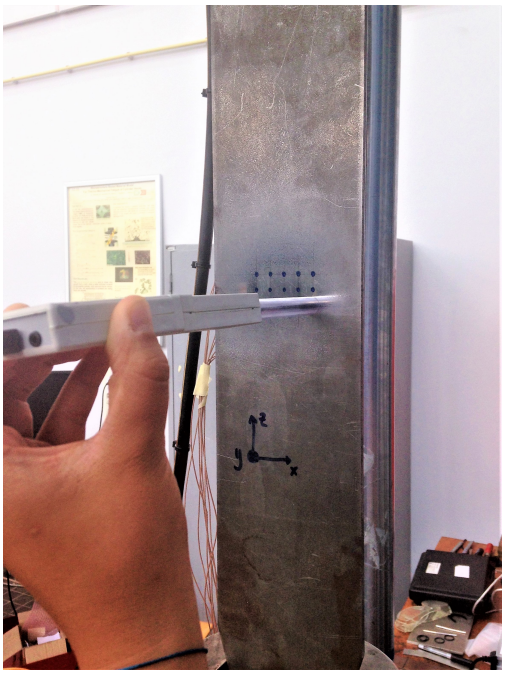

Figure 3.3: Experimental setup SMFL

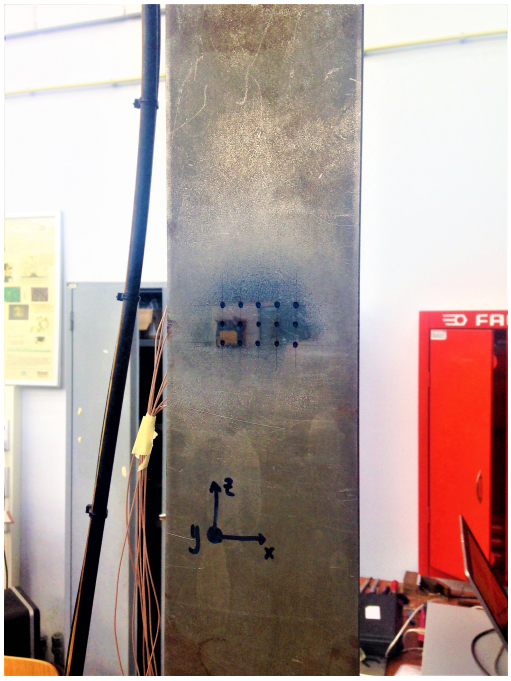

Figure 3.4: The chosen axis and grid

The background field that was measured for this experiment is presented in the table 3.1. This is measured in the area where the experiment takes place.

Axis background field	Magnetic flux density [μT]
x	0
y	-21
z	-33

Table 3.1: Background field experiment SMFL

3.2.3. Parameters fatigue test

The material used is steel with a yield strength of 235 MPa. The specimen is cyclic loaded with a minimum force of 3 kN and a maximum force of 83.5 kN. This results in a mean of 43.5 kN with an amplitude of 40.5 and a load ratio of R=0 as presented in figure 3.5. In appendix B the calculations are presented to insure a crack initiates at the defect.

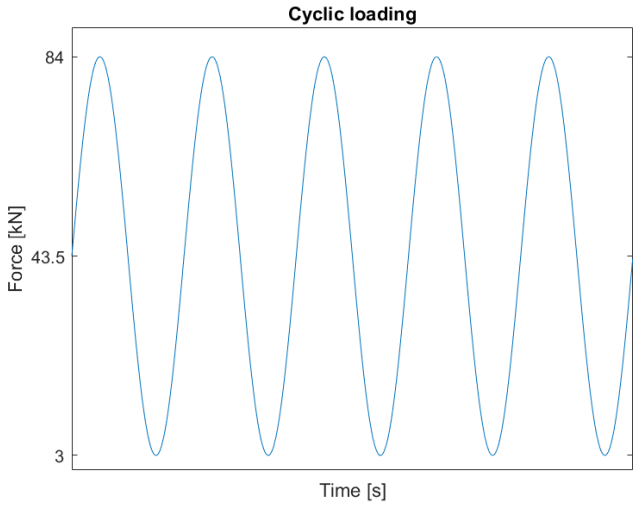

Figure 3.5: Cyclic loading

3.3. Experiment stress-induced magnetization

3.3.1. Geometry

The effect of magnetomechnanical is tested by axially loading the specimen (figure 3.6) for different load levels. The specimen contains a through thickness defect as shown in figure 3.6. The two phenomena of crack opening and the magnetomechanical effect cause a change in the signal strength of the magnetic flux density as explained in section 2.2.3. To solely investigate the contribution of the stresses the difference in crack opening needs to be minimized. A fatigue crack is so small that the crack can be fully closed when there is no stress applied and open when there is. This will result in a relative large contribution of the crack opening effect. With this design the defect is already in an open position and will open slightly more when in tension. This makes it possible to assume that the change in magnetic flux density is caused by the induced stresses according to equation 2.2. The plate is made out of steel with a yield strength of 235 MPa.

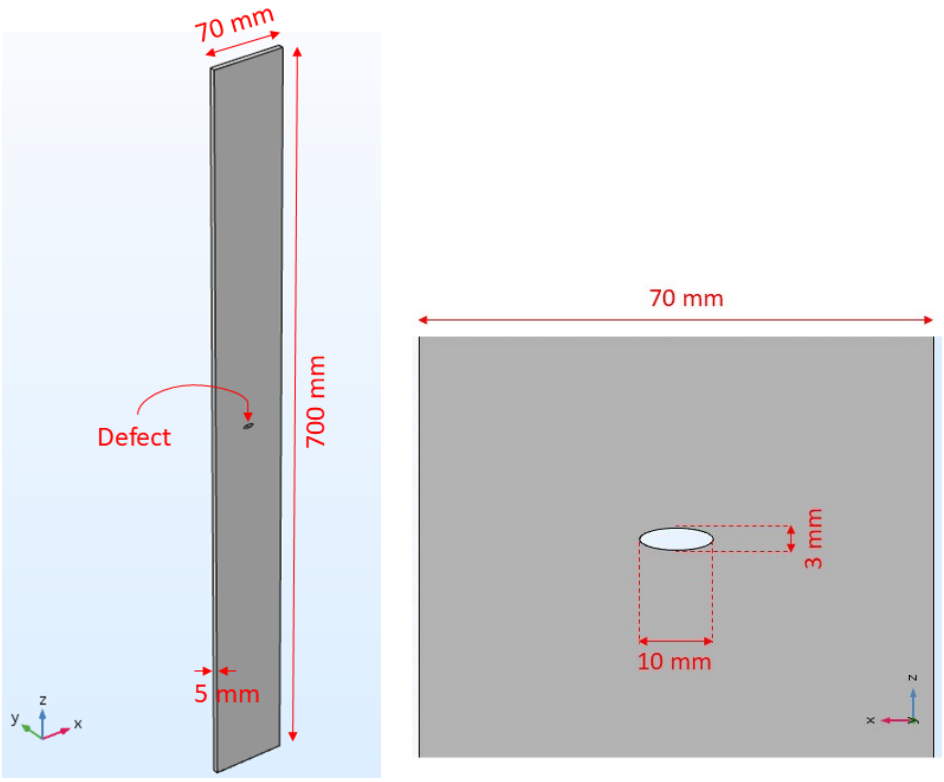

Figure 3.6: Geometry of the specimen with defect for testing the magnetomechanical effect

3.3.2. Experimental Setup

The specimen is loaded by the same MTS machine as described in section 3.2.2 and shown in figure 3.8. In this case the specimen will be statically loaded and this load will increase from 0 to 235 MPa in 40 seconds and will go down to 0 MPa. This process is repeated three times. The force - time diagram for the MTS machine for this experiment is presented in figure 3.7.

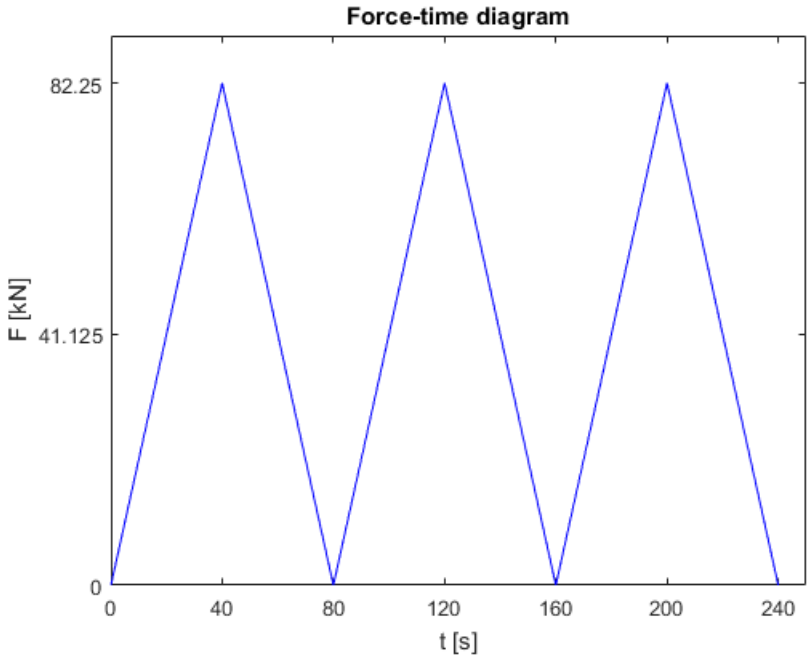

Figure 3.7: Force - time diagram experiment stress-induced magnetization

The magnetic flux density will be measured in y-direction with the same Hall sensor as described in section 3.2.2. The distance between the plate and the probe is kept constant at 1 mm. This is illustrated in figure 3.8 in which the chosen x, y and z axis are shown as well. The measurement of the magnetic flux density will be continuously measured every 0.2 s during the total duration of 3 runs. This is repeated for every grid point in the grid presented in figure 3.9, where the points in z-direction are spaced 4 mm apart and in x-direction 5 mm.

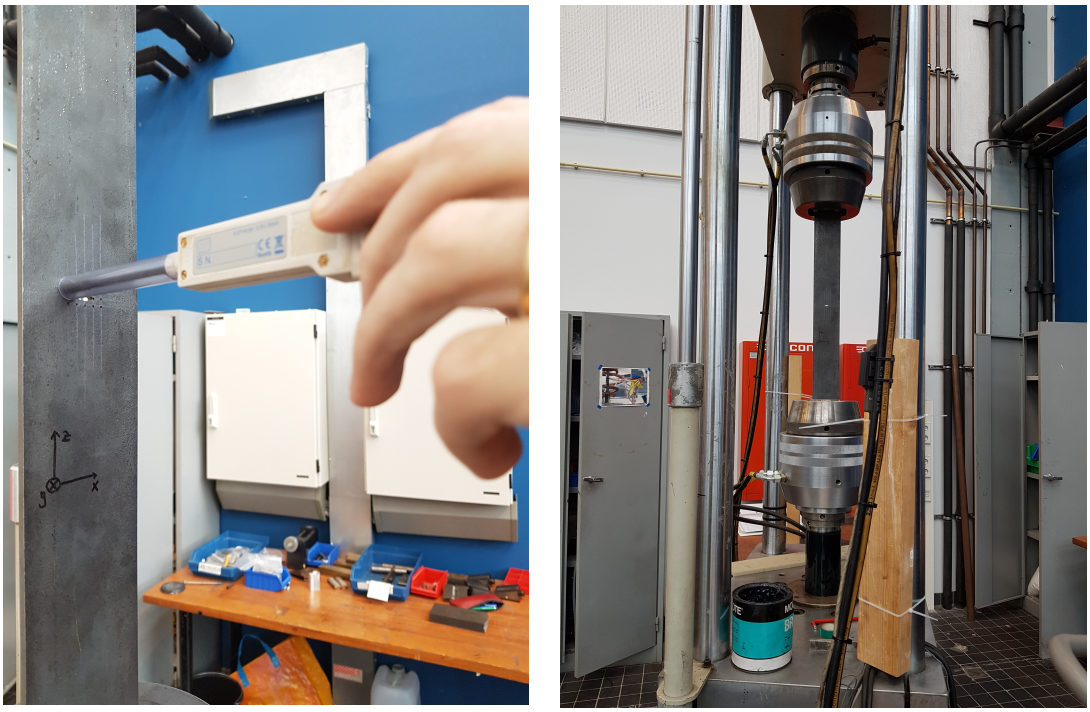

Figure 3.8: Experimental setup

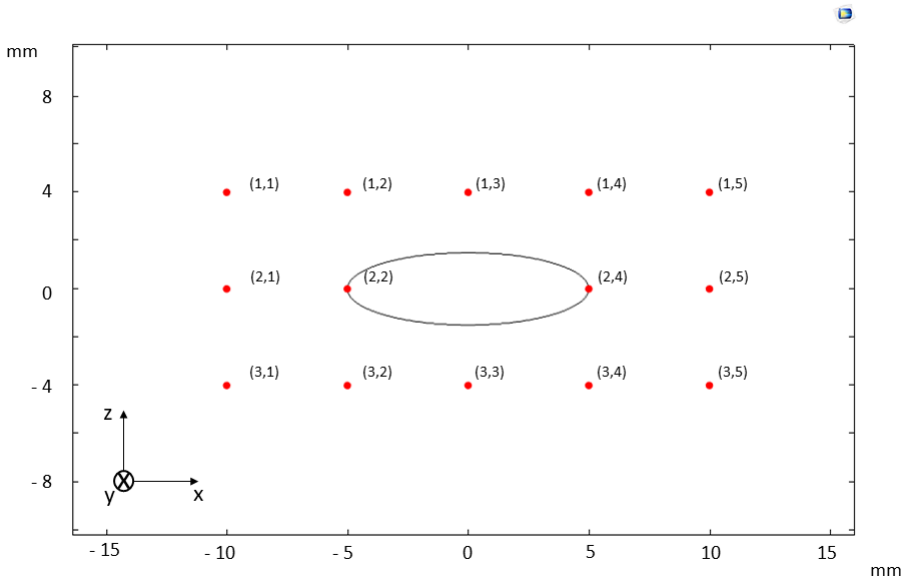

Figure 3.9: Grid experiment stress-induced magnetization

The background field that was measured for this experiment is presented in the table 3.2. This is measured in the area where the experiment takes place.

Axis background field	Magnetic flux density [μT]
x	-10
y	-11
z	-20

Table 3.2: Background field experiment stress-induced magnetization

The measurement for the grid point that shows the highest amount of magnetic flux density will be repeated for 24 cycles to investigate the long-term effects of repeated cyclic loading. The time-force diagram for this case is presented in figure 3.10.

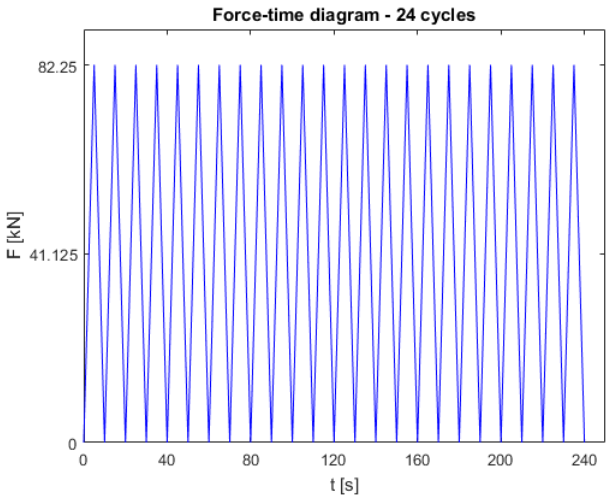

Figure 3.10: Force - time diagram for experiment with 24 cycles

3.4. Follow-up experiment stress-induced magnetization

To investigate the difference in signal for the plastically deformed part and the elastically deformed part a follow-up experiment is carried out. The experiment is repeated in the area of the plate that is not affected by the stress concentration.

3.4.1. Geometry

The same plate is used again in this experiment as described in section 3.3.

3.4.2. Experimental setup

Again, this specimen is loaded in the same manner as described in section 3.3. The only difference in this case is that the loading is reduced in the elastic domain. The force-time diagram for the MTS machine is presented in figure 3.11.

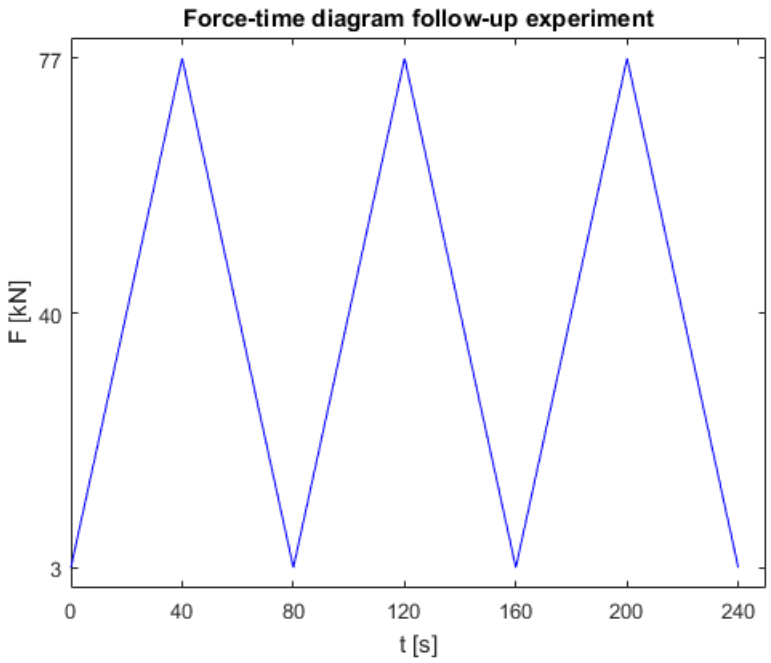

Figure 3.11: Force - time diagram follow-up experiment

The magnetic flux density is measured in the same manner described in section 3.3. The only difference is the extension of the grid into the area of the plate where the stress concentration caused by the defect has no effect anymore. This is located 50 mm above the middle of the elliptically shaped stress concentration. This is shown in figure 3.12 of the experimental setup of the follow-up experiment as well as in figure 3.13 for the extended grid. The new row in the grid is numbered 0. Again, there are 5 points on this row. Point (1,2) and (3,2) of the original grid (3.9) are repeated as reference. The background field during this experiment is presented in the table 3.3. This is measured in the area where the experiment takes place.

Axis background field	Magnetic flux density [μT]
x	-5
y	-14
z	-18

Table 3.3: Background field follow-up experiment

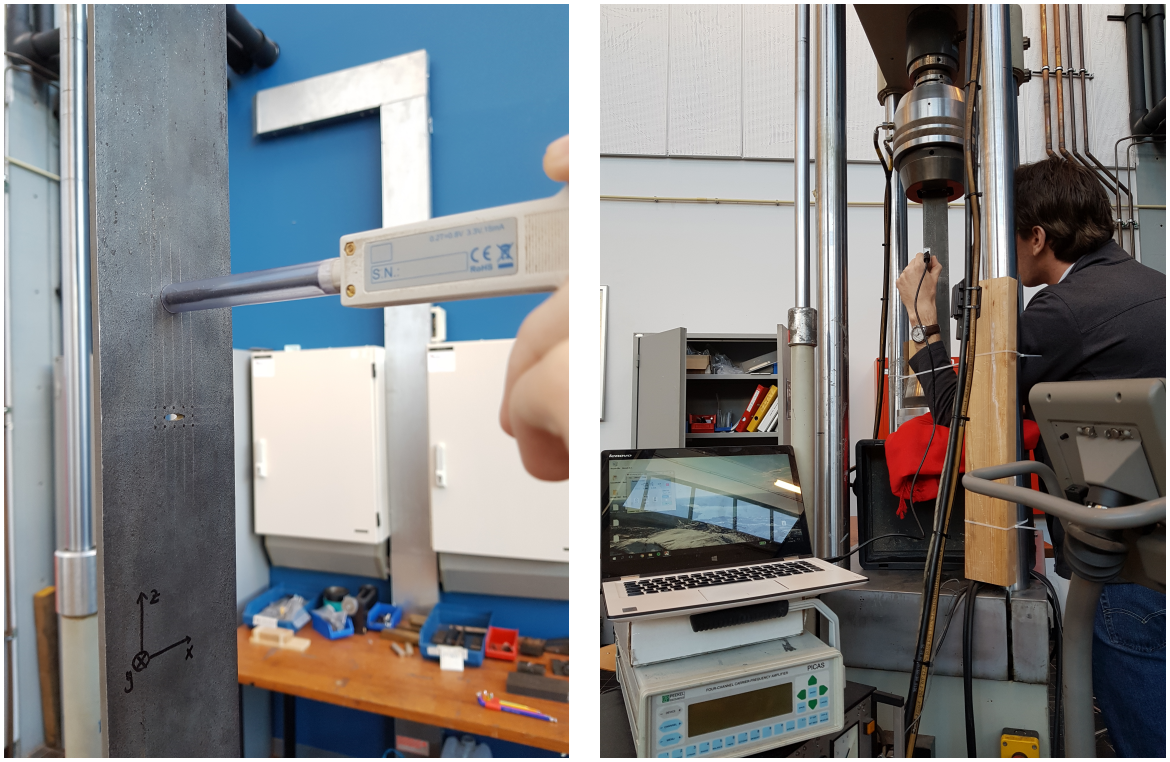

Figure 3.12: Experimental setup follow-up experiment

Figure 3.13: Extended grid for the follow-up experiment

4

Experimental Results

4.1. Introduction

In this chapter the results of the three experiments are presented. The experiments are conducted as explained in chapter 3.

4.2. Results fatigue crack

The results for the experiment measuring the magnetic flux density around a fatigue crack are presented in this section. Figures 4.1, 4.2 and 4.3 show the results for the crack being in an open position. The results for the closed position of the crack are presented in the figures 4.4 and 4.5. In the figures the black dotted line indicates the crack length at the side where the measurements were taken (opposite side from where the defect was made) and the white dotted line indicates the crack at the side where the defect was made.

4.2.1. Open crack

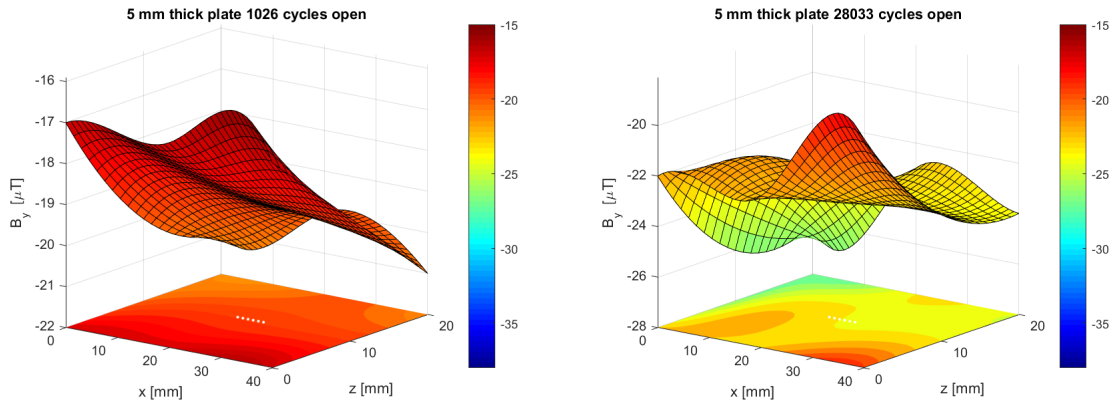

Figure 4.1: B_y for cycles 1026 - 28033 when the crack is open

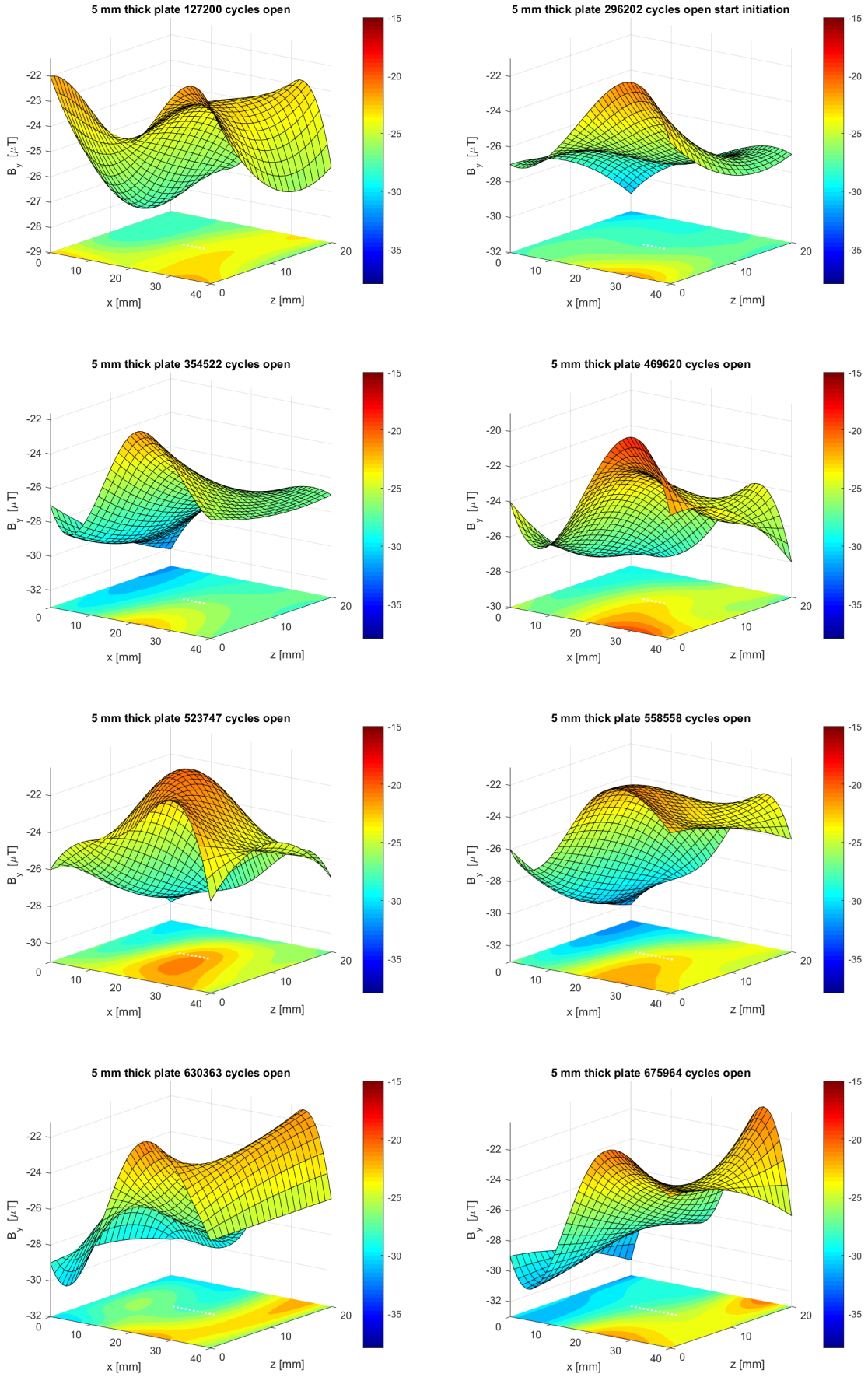

Figure 4.2: B_y for cycles 127200 - 675964 when the crack is open

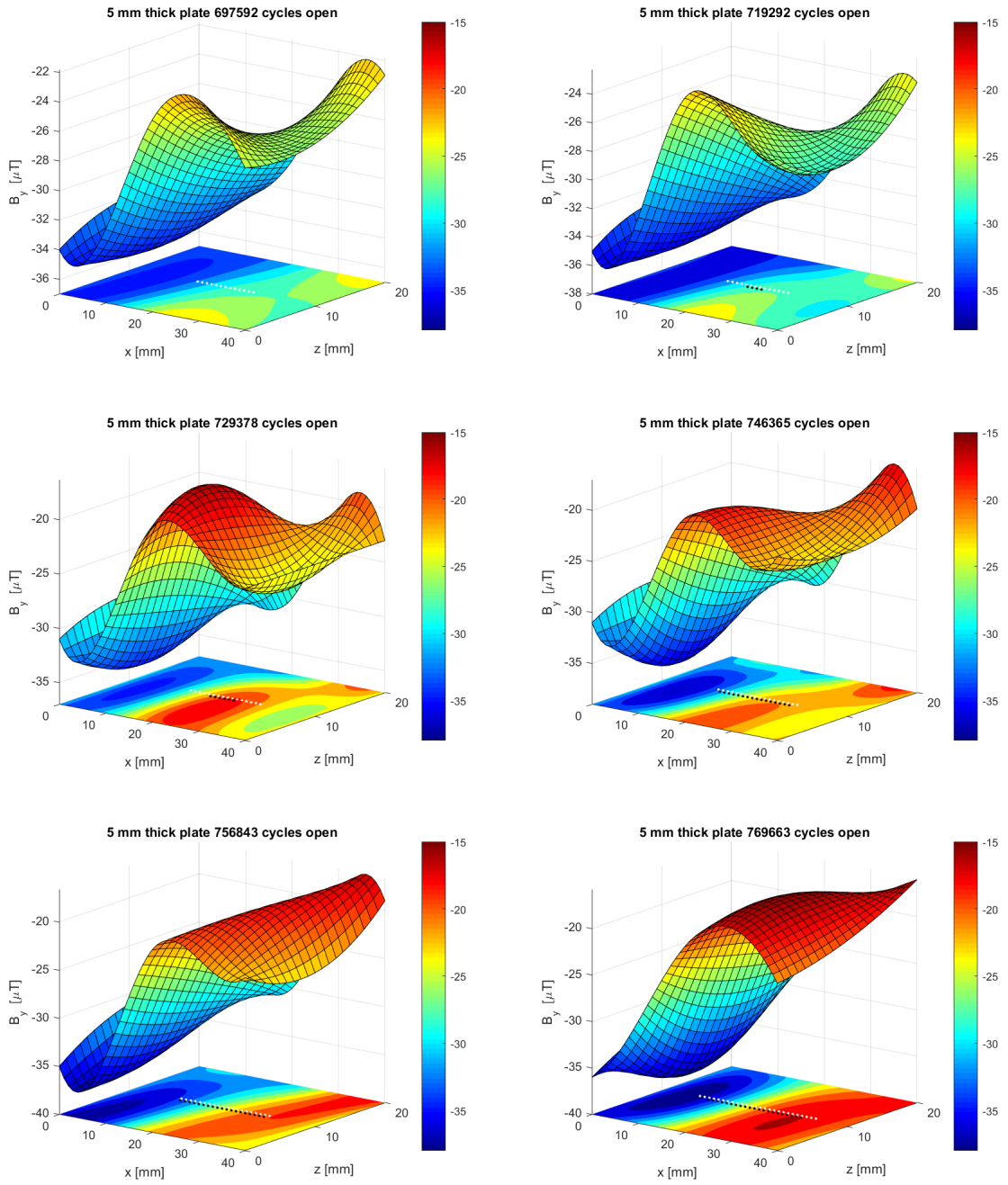

Figure 4.3: B_y for cycles 697592 - 769663 when the crack is open

4.2.2. Closed crack

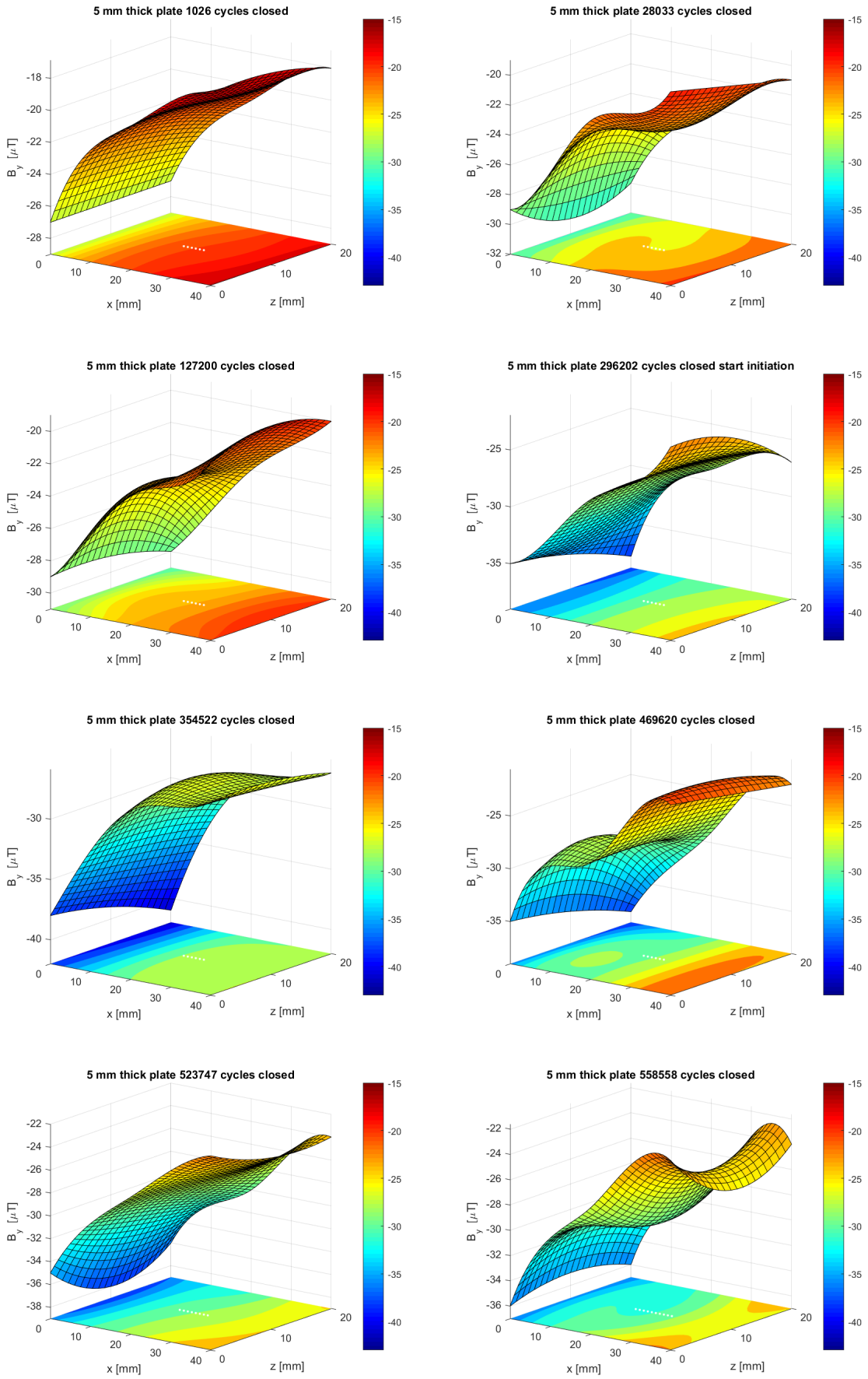

Figure 4.4: B_y for cycles 1026 - 558558 when the crack is closed

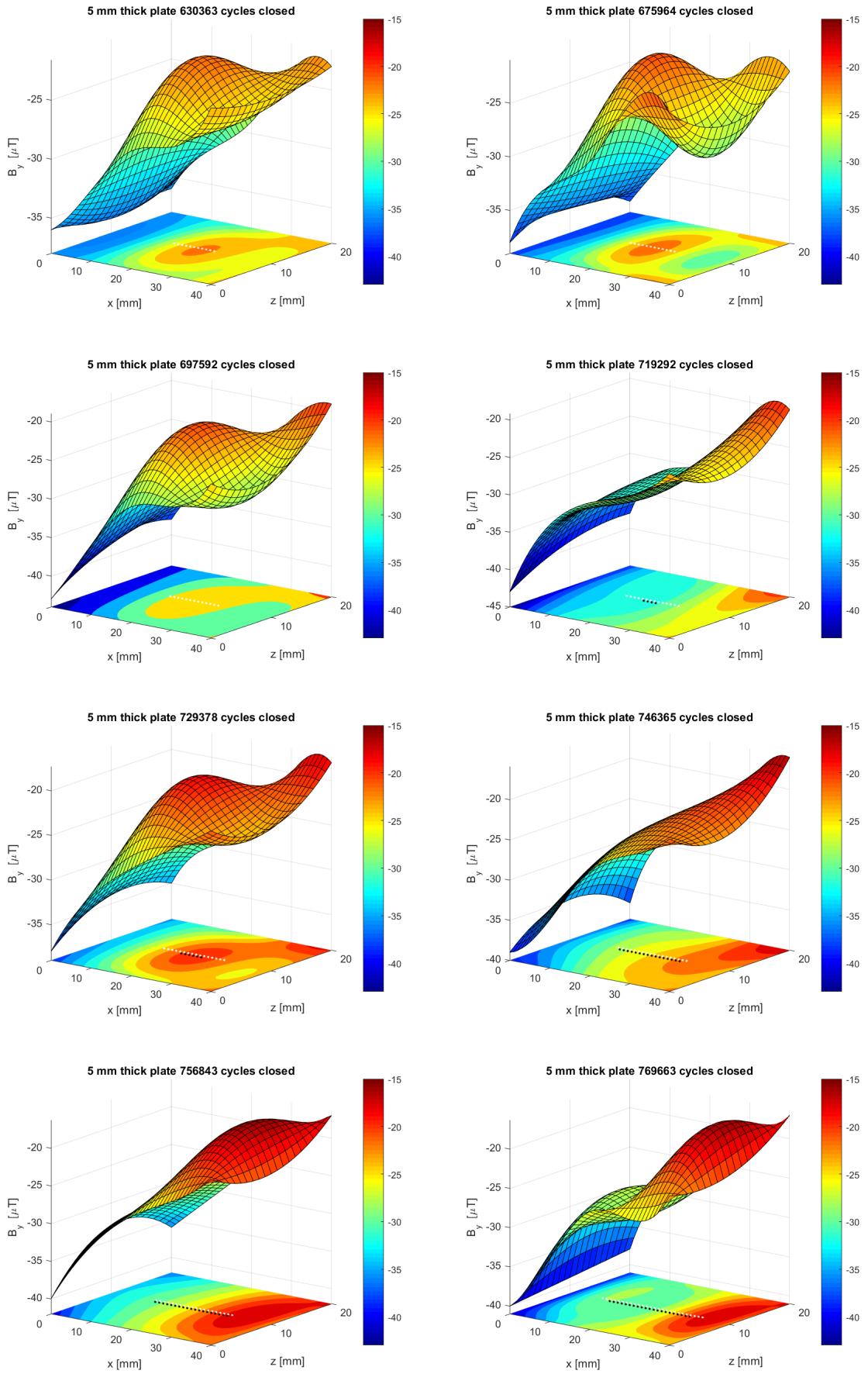

Figure 4.5: B_y for cycles 630363 - 769663 when the crack is closed

4.2.3. Difference open crack

The difference between each measurement is taken for the results with an open crack, to see how the magnetic flux density changes when the crack propagates. To do so every measurement is subtracted with the measurement before that was done before: measurement(i) – measurement(i-1).

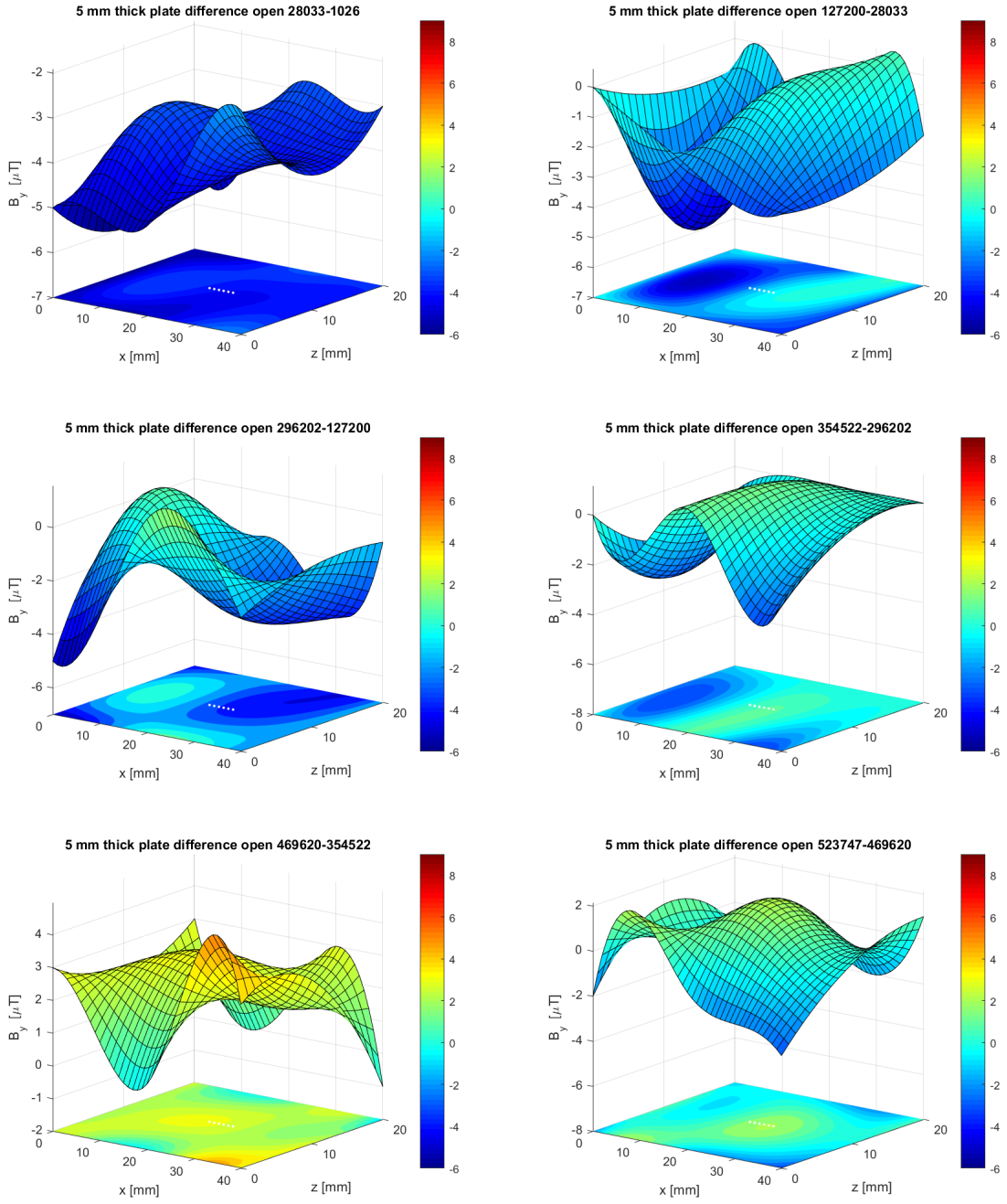

Figure 4.6: Difference in B_y for cycles 1026 - 630363 when the crack is open

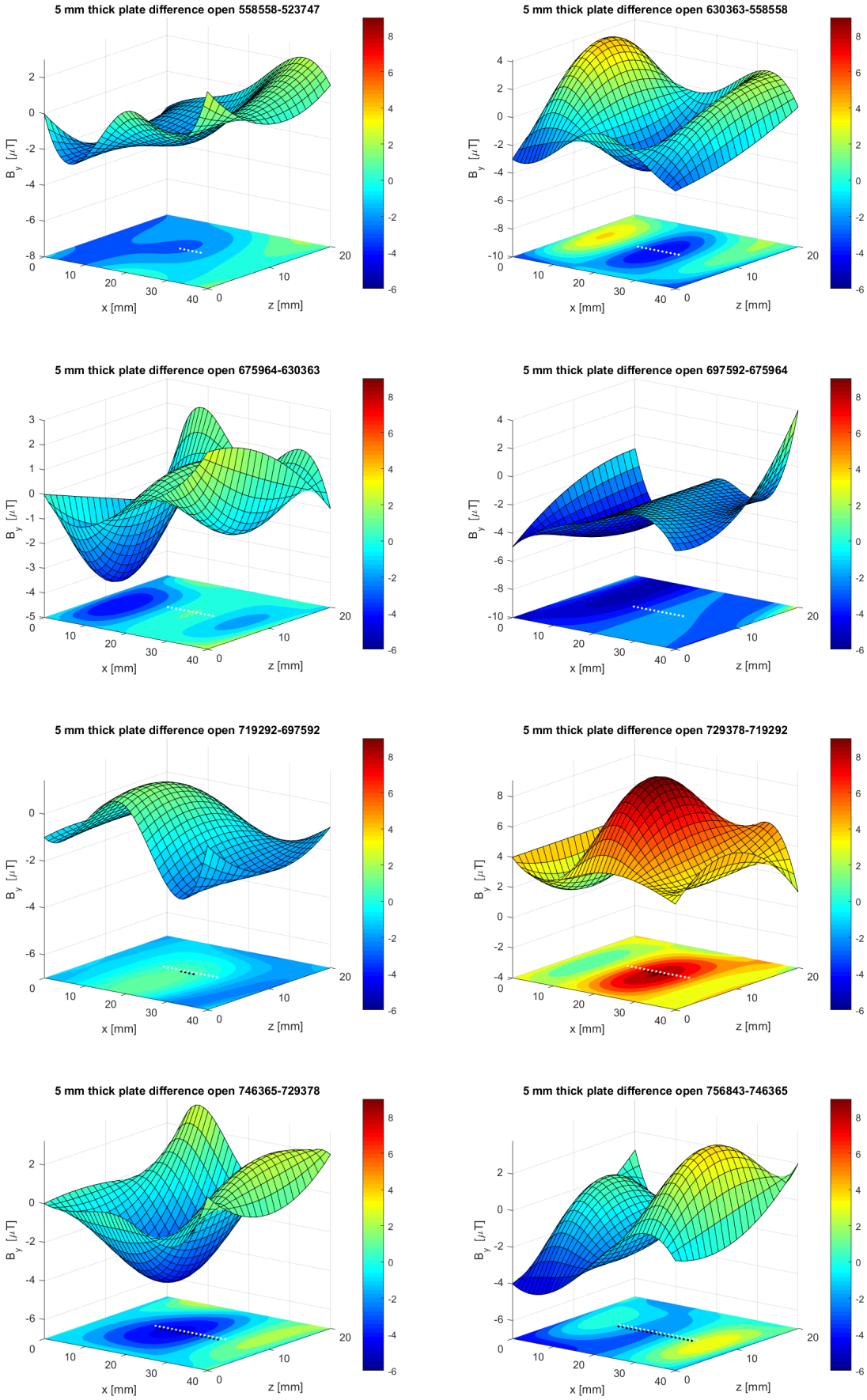

Figure 4.7: Difference in B_y for cycles 675964 - 756843 when the crack is open

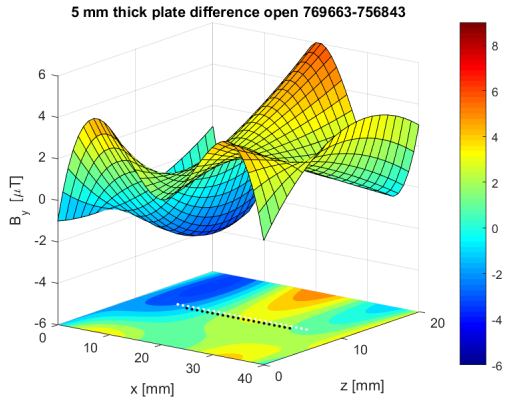

Figure 4.8: Difference in B_y for cycle 769663 when the crack is open

4.2.4. Difference open and closed crack

The difference in magnetic flux density is plotted for the crack being in open and closed position. This is plotted for every measurement in the figures 4.9, 4.10 and 4.11.

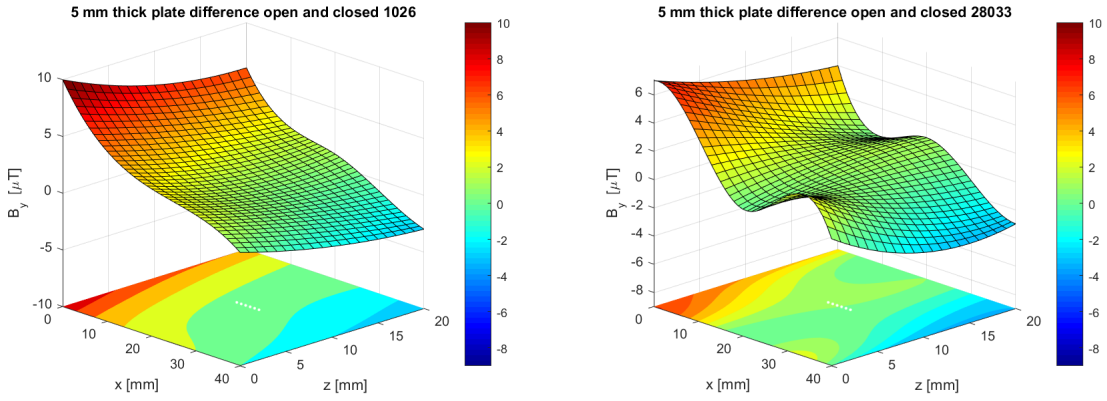

Figure 4.9: Difference in B_y for cycles 1026 - 28033 between the crack being open and closed

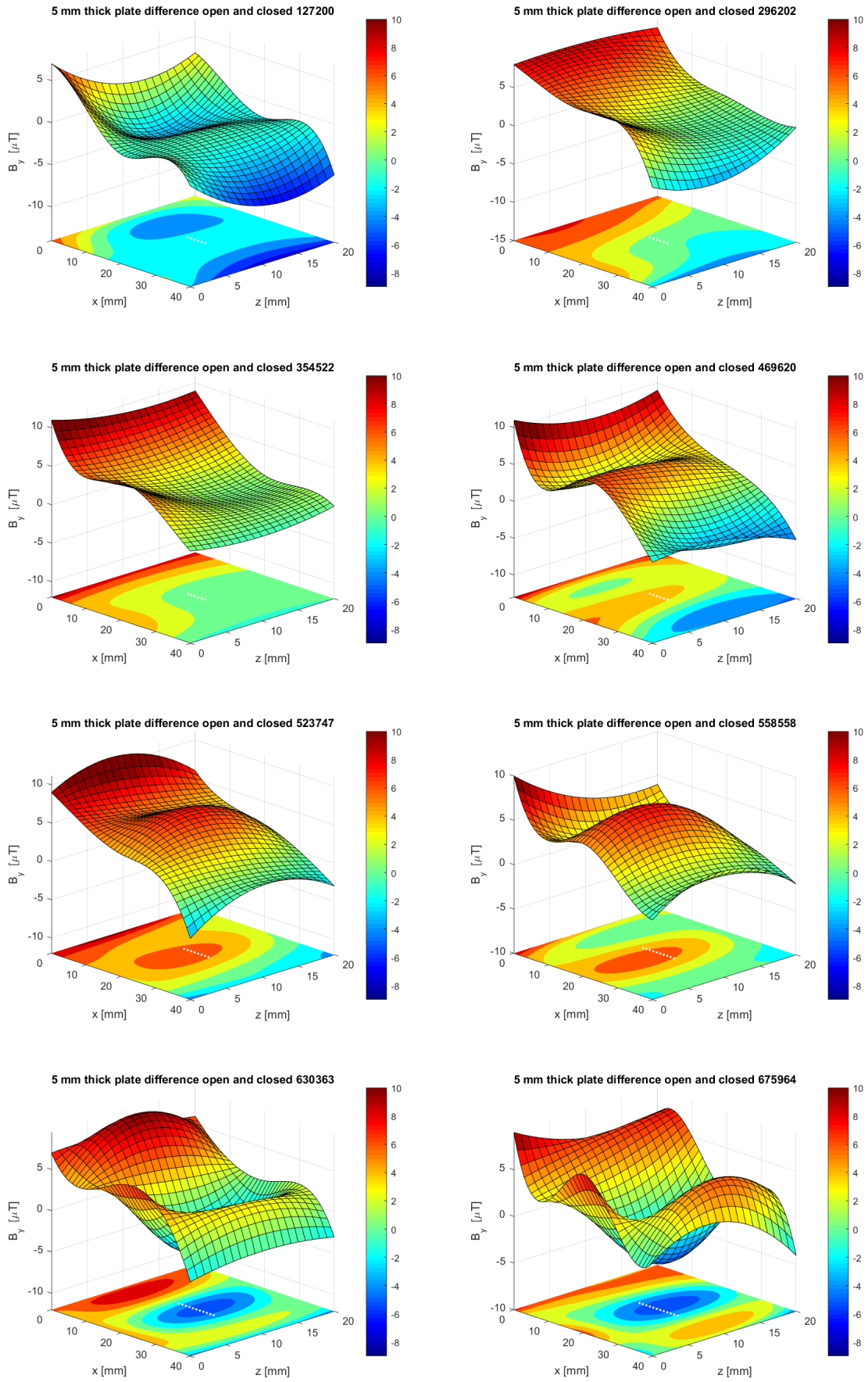

Figure 4.10: Difference in B_y for cycles 127200 - 675964 between the crack being open and closed

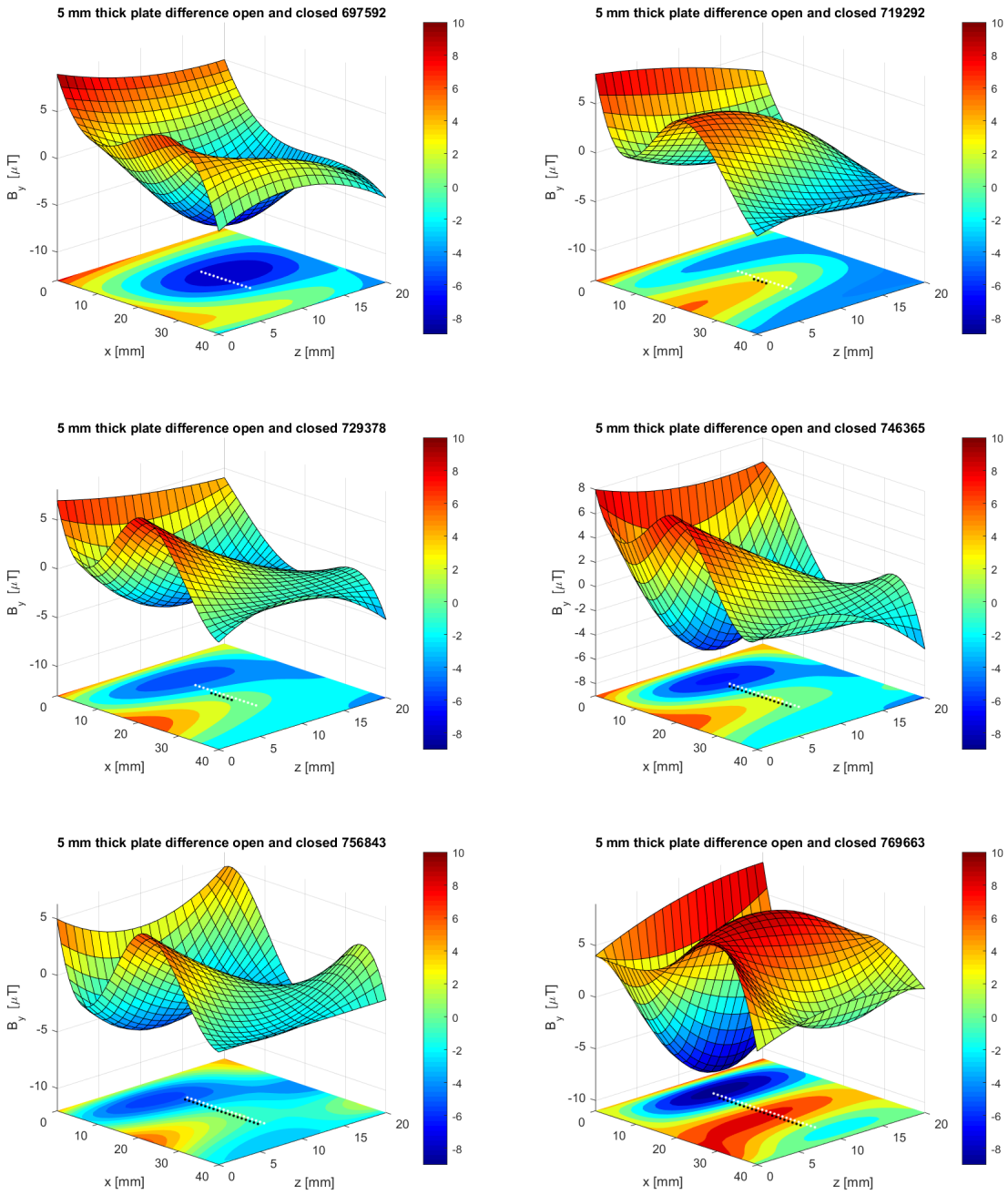

Figure 4.11: Difference in B_y for cycles 697592 - 769663 between the crack being open and closed

4.3. Results stress-induced magnetization

In this section the results for the experiment described in section 3.3 are presented.

4.3.1. Raw Data

In this section the results of the experiment for determining the stress-induced magnetization are presented. In the figures 4.12, 4.13 and 4.14 the raw data is presented for row 1, 2 and 3 of the grid as shown in figure 3.9.

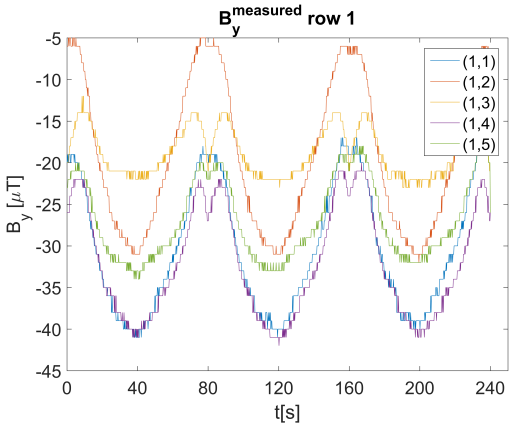

Figure 4.12: B_y row 1

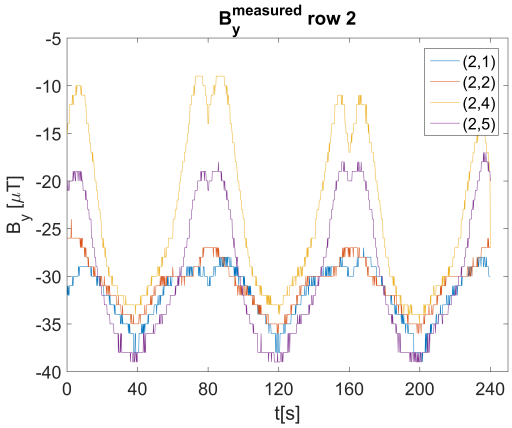

Figure 4.13: B_y row 2

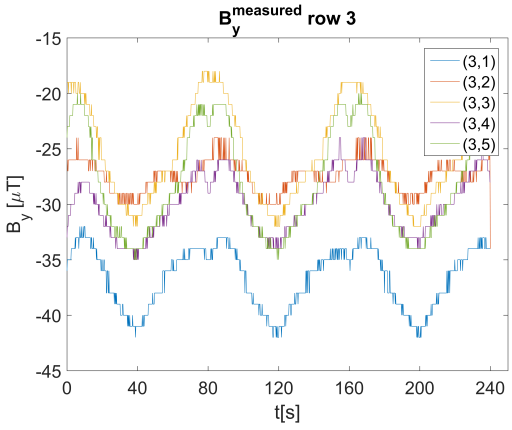

Figure 4.14: B_y row 3

4.3.2. Change induced by stress

As explained in section 2.2.3 the magnetic flux consist of three components: the induced magnetism, the permanent magnetism and the magnetization induced by the stresses in the material. It is assumed that the surrounding field does not change during the experiment. This means that the induced magnetism can be assumed constant and can be modeled in a Finite Element Model which is done in chapter 5. The permanent magnetization at a specific point in the material is assumed constant. In this experiment these locations are chosen according to the grid in figure 3.9. This results in the stress-induced magnetization being the only factor that changes during loading. At $t = 0$ it is assumed that magnetic flux density measured corresponds to the induced and permanent magnetism according to equation 2.2. This value is subtracted from all the raw data

$$B_y^\sigma(t) = B_y(t) - B_y(t=0) \tag{4.1}$$

and results in the change of magnetic flux density due to the induced stresses. This is presented in figures 4.15, 4.16 and 4.17 for row 1, 2 and 3 . In these figures the low-pass filter, moving average, was used to reduce the perturbations in the signal and increase the readability. This filter, filters coefficients equal to the reciprocal span [9]. In this case a reciprocal span of 15 was chosen and figure 4.18 shows that the perturbation are correctly filtered out of the data.

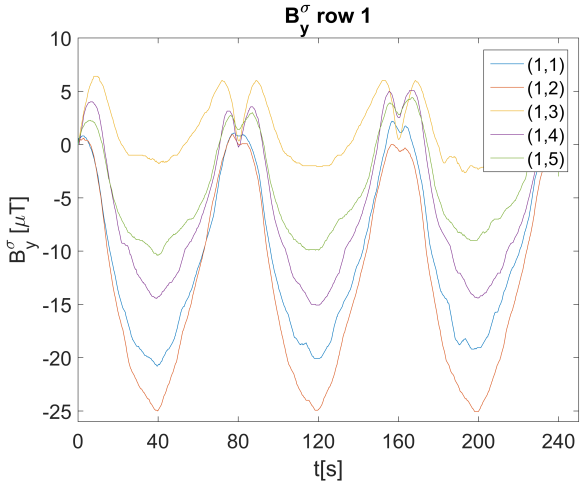

Figure 4.15: ΔB_y row 1

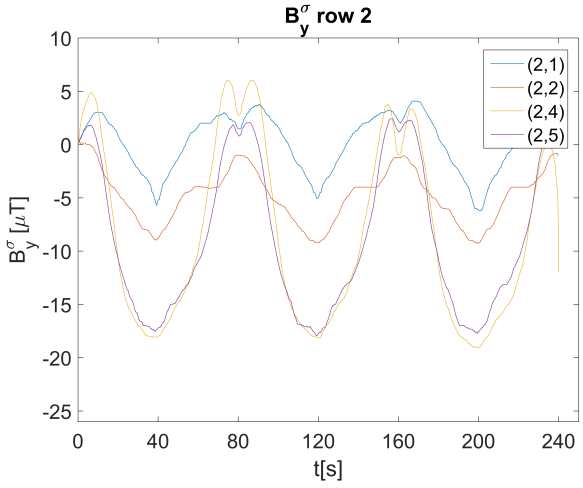

Figure 4.16: ΔB_y row 2

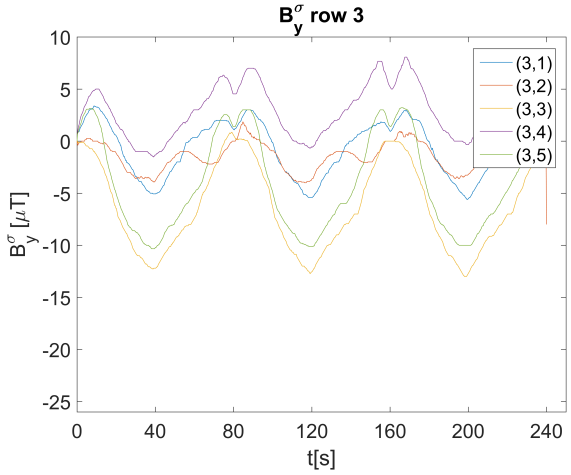

Figure 4.17: ΔB_y row 3

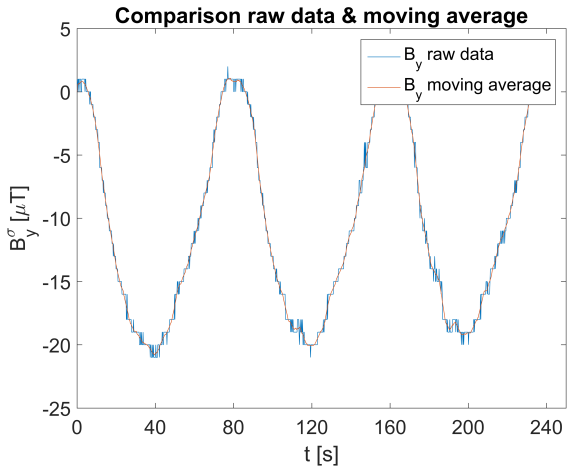

Figure 4.18: Filtered vs. raw data

The stresses are symmetrically distributed in the plate around the elliptical hole. To investigate if the stress-induced magnetization also is symmetrically distributed, the grid points (1,1), (1,5), (3,1) and (3,5) are compared in figure 4.19.

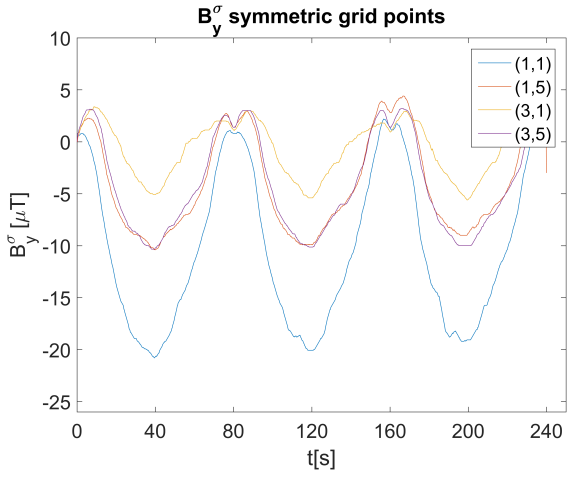

Figure 4.19: Symmetric grid points stress-induced magnetization

4.3.3. Hysteretic effects

To investigate if the stress magnetization is a hysteretic effect, the applied force is plotted against the difference in magnetic flux density for every point of the grid (figure 3.9). There are 6 different periods for the force. This can be seen in figure 3.7, 3 periods up when the force increases and 3 periods down when the force decreases. The datasets plotted in figures 4.15, 4.16 and 4.17 are split in these six periods and are plotted for the force that was applied on the specimen. This is presented in figure 4.20 and shows the six periods. To analyse the hysteretic behavior, the results are averaged over the three periods for an increasing force and decreasing force. The plots for every grid point are presented in figures 4.21, 4.22 and 4.23.

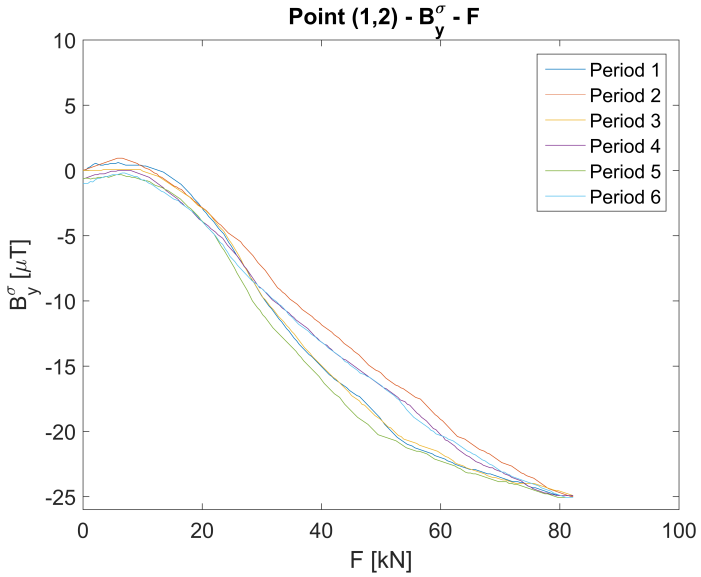

Figure 4.20: ΔB_y - force diagram

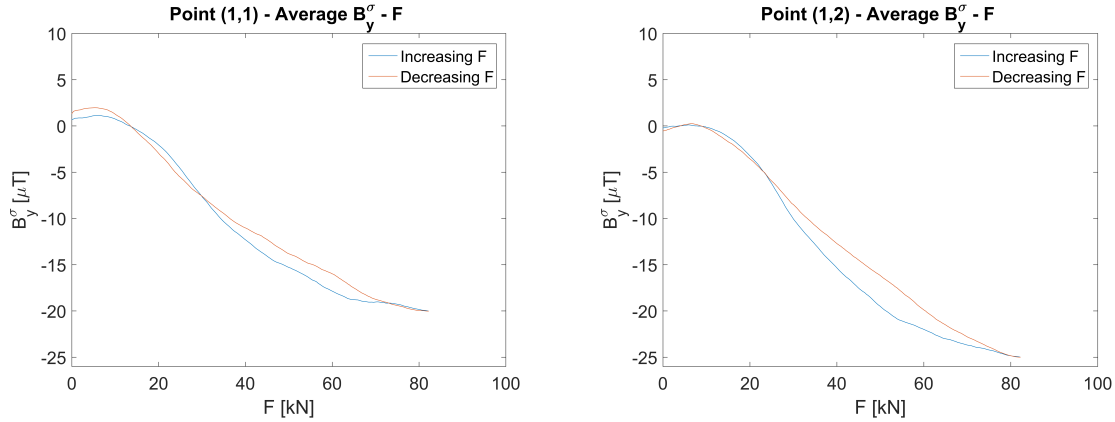

Figure 4.21: Average ΔB_y - force diagram point (1,1) to (1,2)

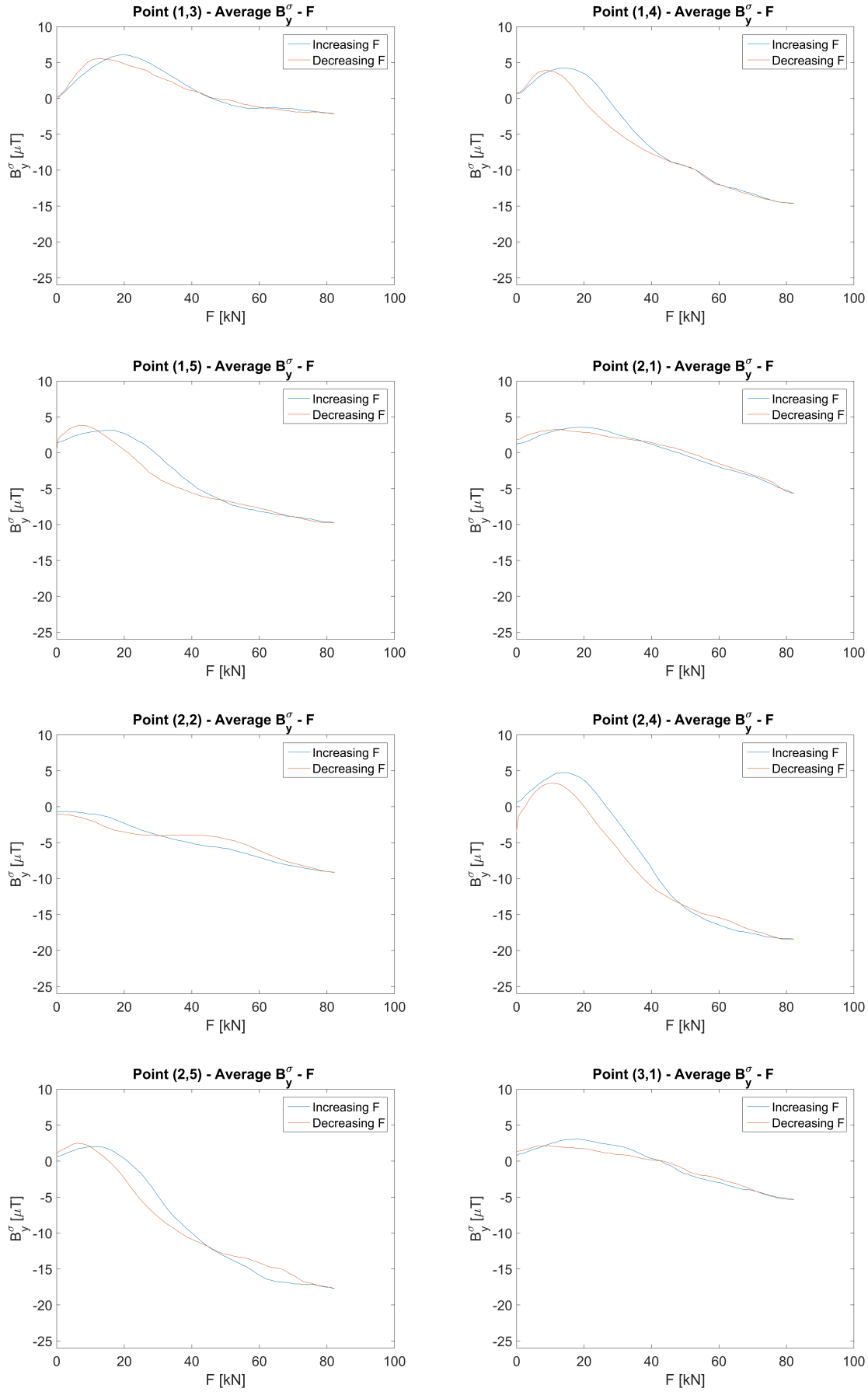

Figure 4.22: Average ΔB_y - force diagram point (1,3) to (3,1)

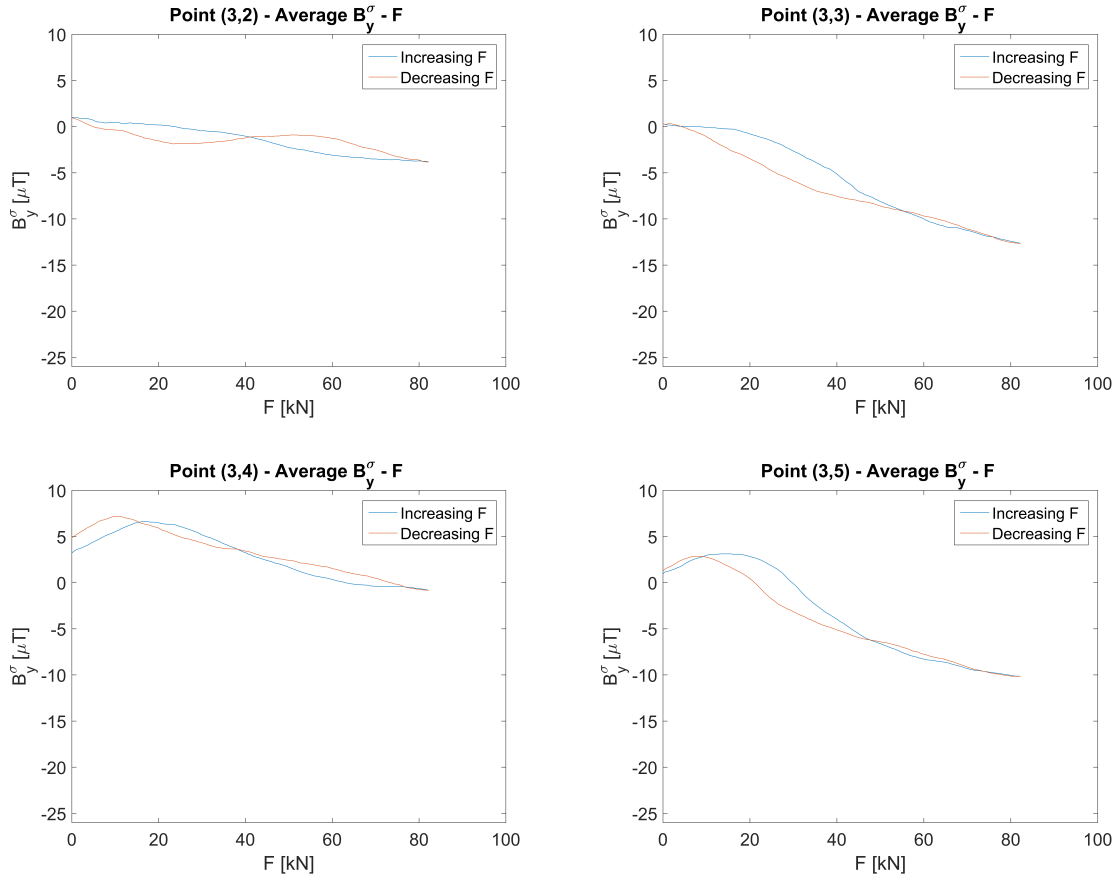

Figure 4.23: Average ΔB_y - force diagram point (3,2) to (3,5)

The hysteretic effects for point (1,2) and (1,3) are combined in one plot to see the difference between the neutral line (point (1,3)) and a point next to it (point (1,2)) and this is shown in figure 4.24.

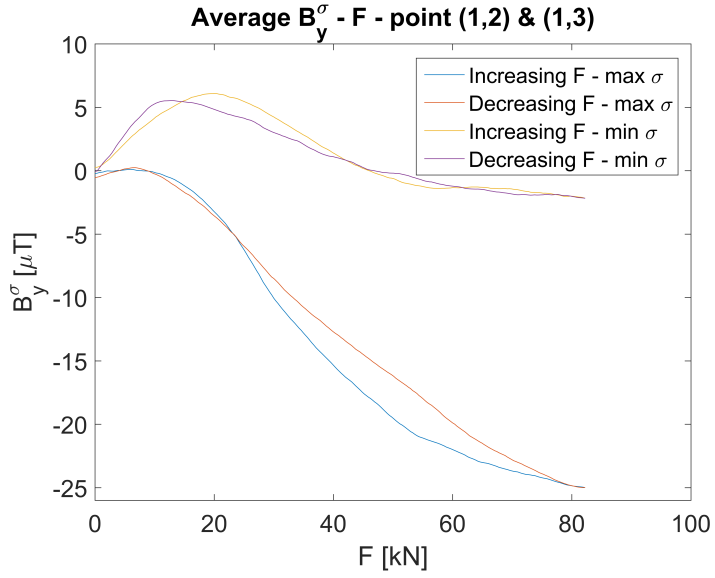

Figure 4.24: Neutral line vs stressed area

4.3.4. Long-term effects of cyclic loading

After all the measurements were done in the grid 3.9, point (1,2) was repeated to investigate the long-term effects of cyclic loading as described in section 3.2.2. Three cycles at the start of this measurement and three cycles at the end of this measurement are compared to the original data from point (1,2) presented in figure 4.16. The results are shown in figures 4.25 and 4.26.

For this dataset the hysteretic effect was investigated again by splitting the dataset into 24 periods where the force was increased and 24 periods where the force was decreased. The average of the 24 periods were taken, resulting in the hysteretic curve presented in figure 4.27.

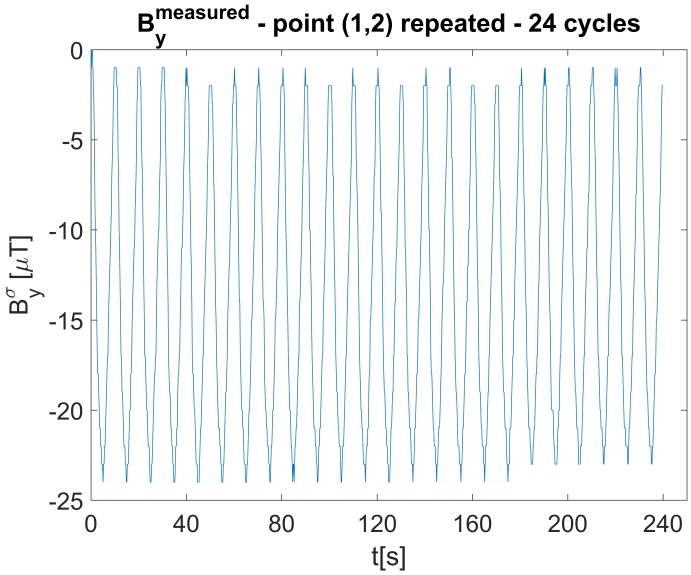

Figure 4.25: Measurement point (1,2) repeated with 24 cycles

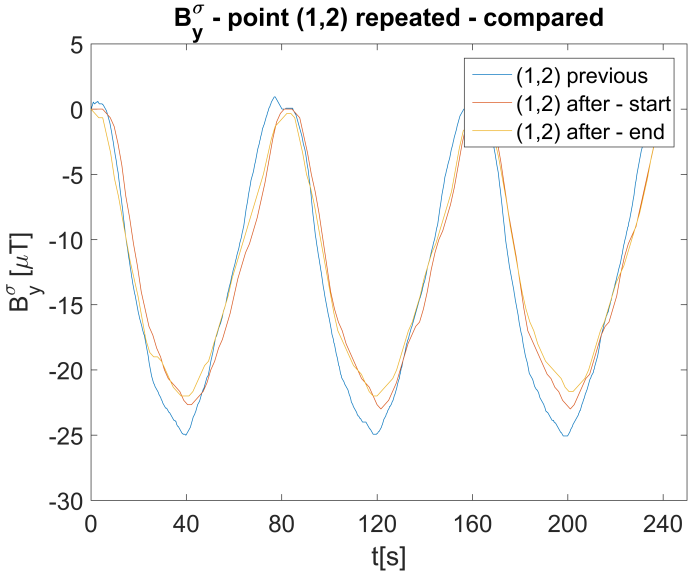

Figure 4.26: Measurement point (1,2) repeated and compared to previous measurement

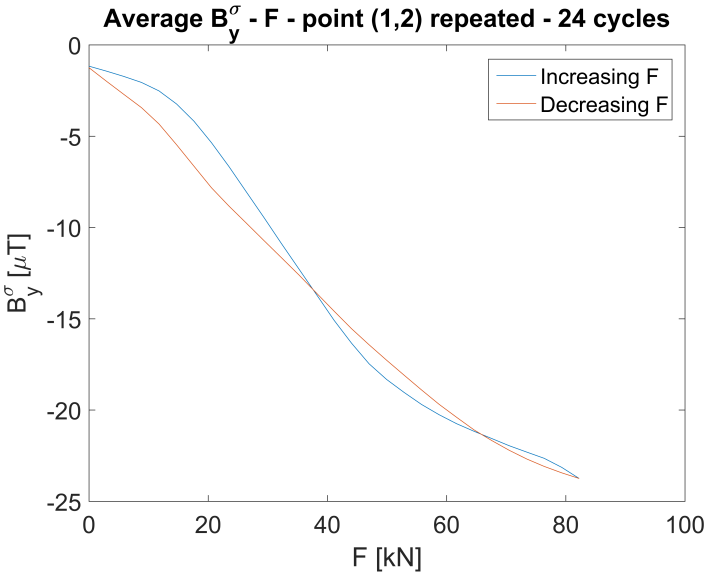

Figure 4.27: Average ΔB_y - force diagram point (1,2) repeated with 24 cycles

4.4. Results follow-up stress-induced magnetization

In this section the results for the follow-up experiment are presented as described in section 3.4. This experiment investigates the effect of the stress-induced magnetization without the effect of plastic deformation around a stress concentration.

4.4.1. Raw Data

In the figures 4.28 the raw data is presented for row 0.

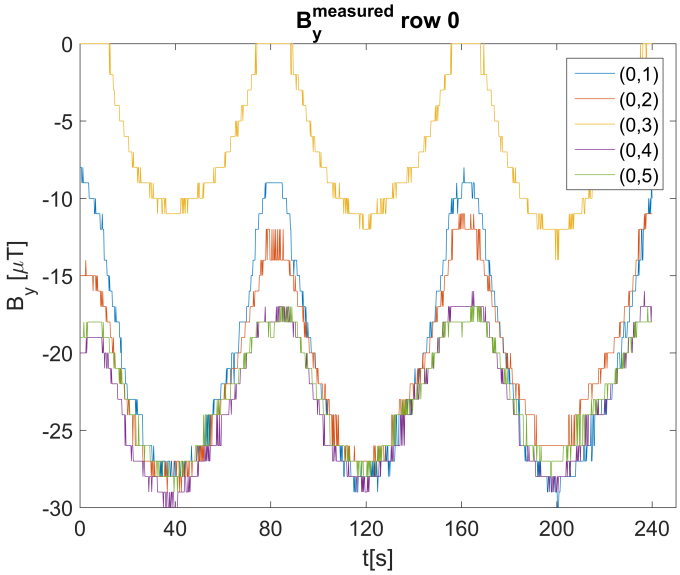

Figure 4.28: B_y row 0

4.4.2. Change induced by stress

As explained in section 4.3.2 the difference in B_y is plotted by subtracting B_y at t = 0 from the results. In this case the data is also filtered with a moving average with a reciprocal of 15.

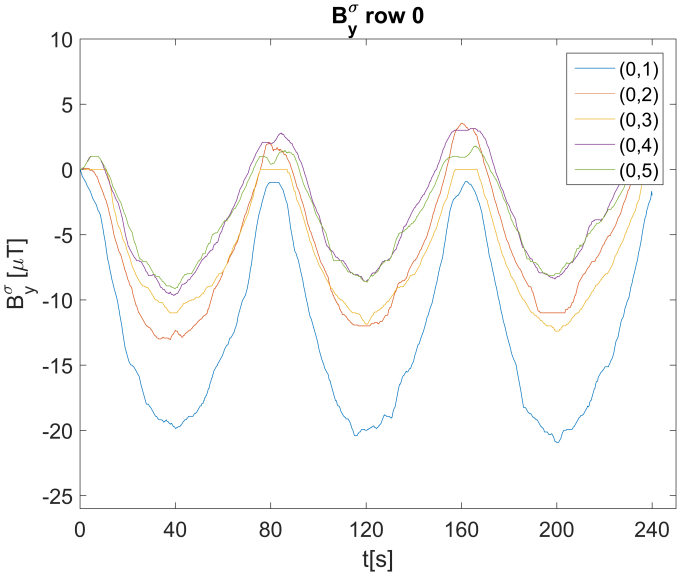

Figure 4.29: ΔB_y row 0

4.4.3. Hysterese effects

The hysteretic effects are investigated by taking the average of the three periods when the force increases and decreases as described in section 4.3.3. The plots for every grid point are presented in figure 4.30,

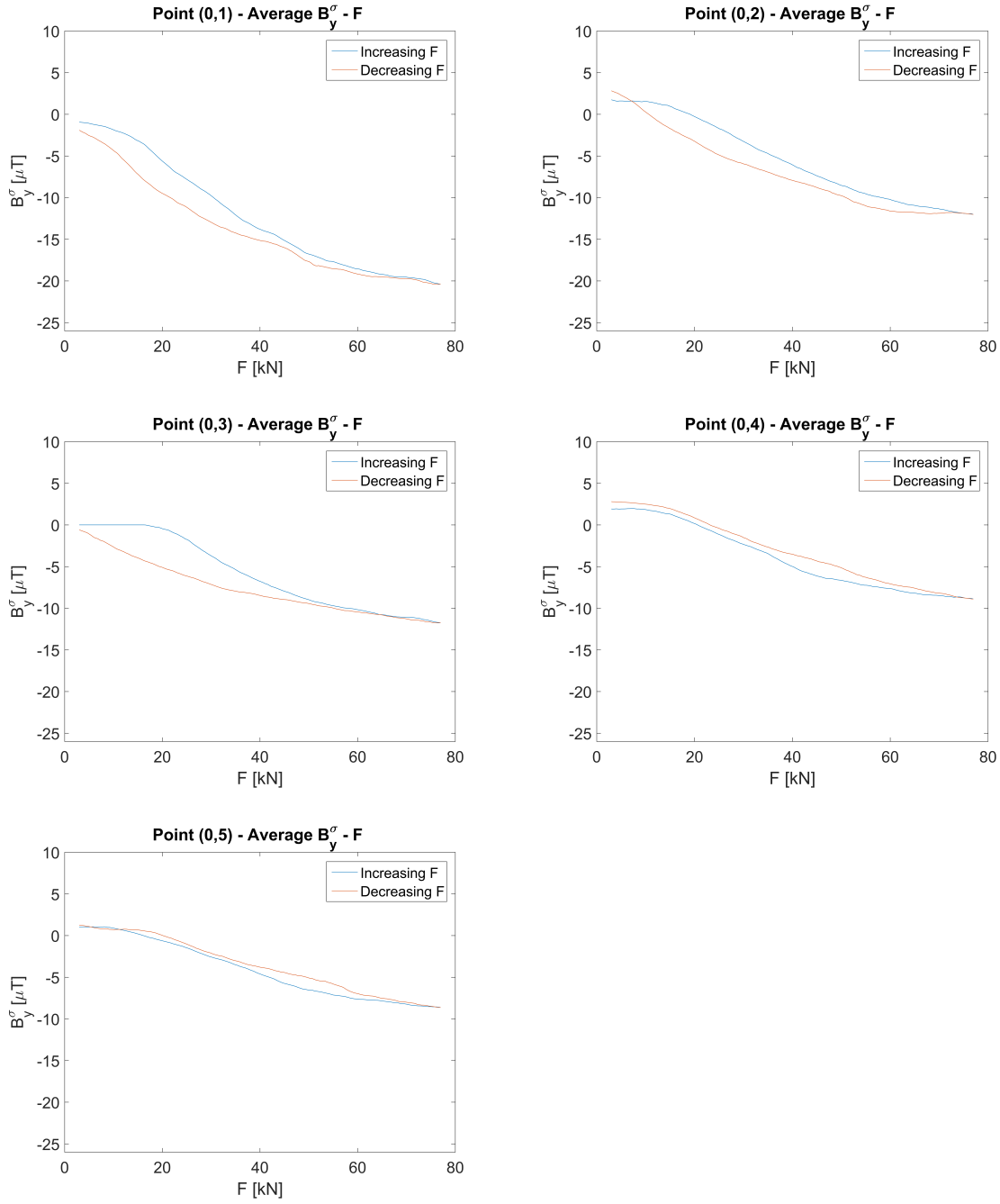

Figure 4.30: Average ΔB_y - force diagram point (0,0) to (0,5)

4.4.4. Effect of plastic deformations

The grid points (1,2) and (3,2) are measured again to investigate the difference between the area affected by plastic deformation and the area affected only by elastic deformation. These results are obtained according to section 3.4 and presented in figure 4.31.

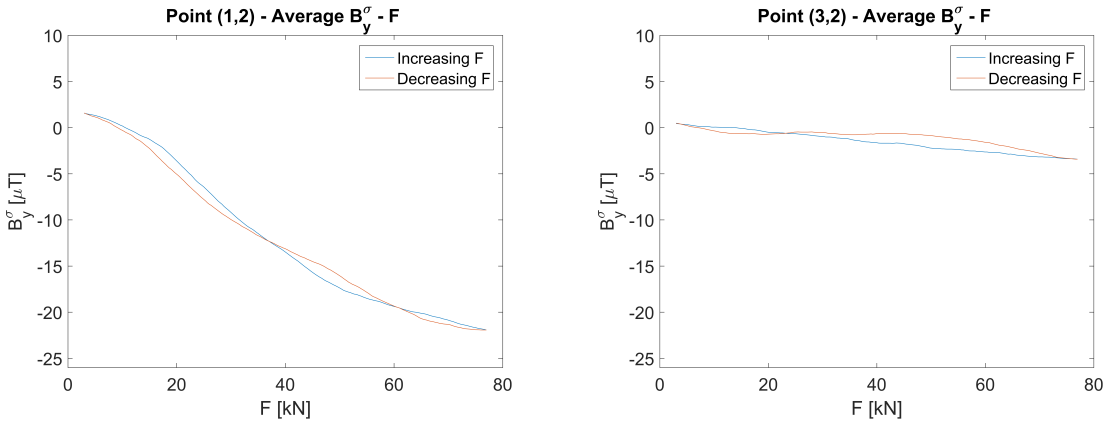

Figure 4.31: Average ΔB_y - force diagram point (1,2) and (3,2)

5

Numerical Simulation

5.1. Introduction

To get more insight in the experimental results numerical simulations were done. The Finite Element Method (FEM) software package used for this is COMSOL Multiphysics. It needs to be taken into account that the permanent magnetism cannot be modeled in a FEM model. This is due to its hysteretic behavior and the inhomogeneous distribution in the material as described in section 2.2.3. This means that there always is a discrepancy between a FEM model and the experimental results.

5.2. Magnetic model - fatigue crack

Geometry

The geometry is modeled in COMSOL Multiphysiccs as shown in 3.1 with a box of air around it of 15 x 15 x 15 m (L x B x H). The geometry of the defect is modeled as an through thickness crack with a width of 20 mm and an opening of 0.1 mm as shown in figure 5.1. The results were obtained for the same area as the grid described in section 3.2. The grid in the model consists of 42 vertical lines spaced 1 mm between each other as presented in figure 5.1.

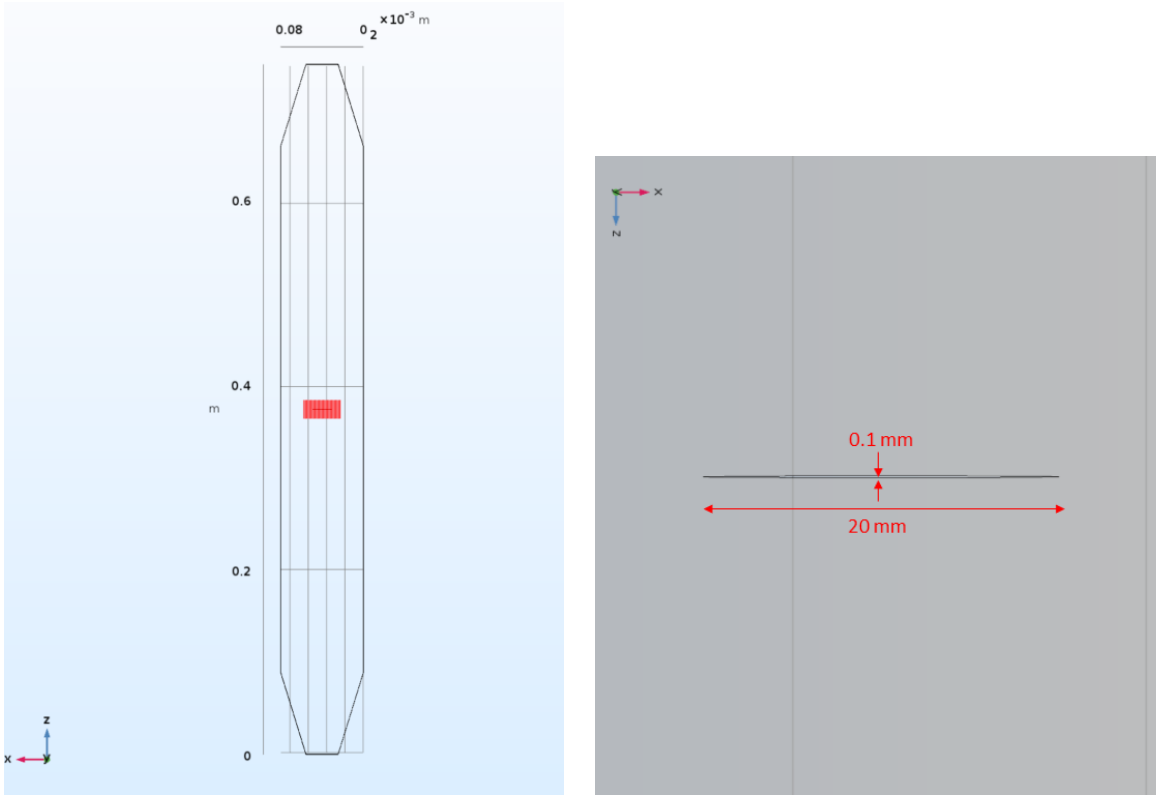

Figure 5.1: Grid used in COMSOL Multiphysics and geometry defect

Materials & Meshing

Since only weak fields are being considered, hysteresis effects were disregarded and the steel material of the plate was modeled linearly with a relative permeability of 225 [27]. The other material used in these models is air, with a relative permeability of 1. The model was meshed using free tetrahedral meshing.

Boundary conditions

The magnetostatic solver used in this model is 'Magnetic Fields, No Currents' in COMSOL Multiphysics and the results are conducted for a stationary study. The background magnetic field was set as in table 3.1. The boundary condition 'Magnetic Flux Conservation' was set for the domain of the steel plate. The 'External Magnetic Flux Density' boundary condition was used for the outer boundaries of the box of air.

Results

The magnetic flux density in y-direction is calculated for every point on the red lines. These values were interpolated with Matlab to increase readability since the crack has an opening of only 0.1 mm. This result is presented in figure 5.2. The white dotted line in the figure indicates the crack.

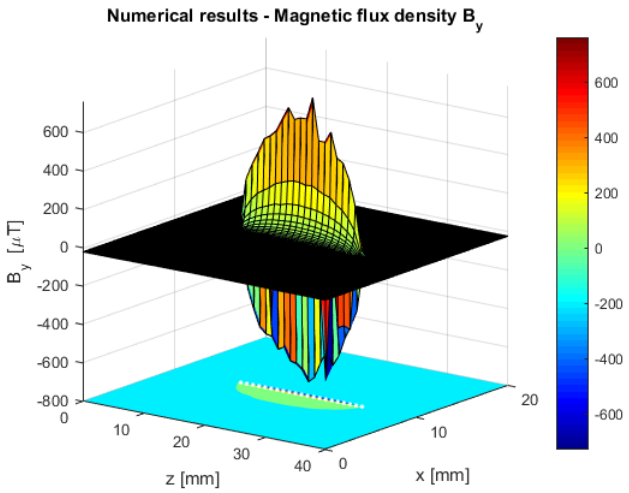

Figure 5.2: Numerical results B_y for fatigue crack

5.3. Stress model - fatigue crack

The experimental results do not correspond to the results from the FEM model. This is explained in more detail in chapter 6. The literature in section 2.2.3 suggest differences in the magnetic signal due to the induced stresses. For that reason a FEM model in COMSOL Multiphysics is built to calculate the stresses in the material.

Geometry

The same grid is used as described in figure 5.1. The geometry for the stress model is an adjustment of the geometry in figure 5.1. The geometry is cut off were the machine clamped the specimen and exerted the force on it. This is shown in figure 5.3

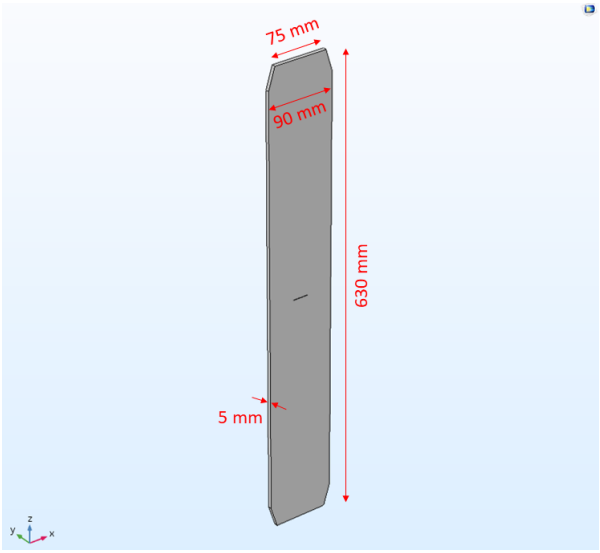

Figure 5.3: Geometry used in the stress model

Materials & Meshing

The material that was used to model the steel plate is the predefined material 'Structural Steel' with a E-modulus of 200 GPa in COMSOL Multiphysics. The model was again meshed using free tetrahedral meshing.

Boundary conditions

The solver used in this model is 'Solid Mechanics' in COMSOL Multiphysics and the results are conducted for a stationary study. The boundary condition 'Fixed Constraint' was set for the lower end of the plate. The condition 'Boundary Load' was set at a load of 84000 N in positive z-direction for the top boundary of the plate.

Results

The Von Mises stresses are calculated for every point on the red lines. These values were again interpolated with Matlab to increase readability. This result is presented in figure 5.2. The white dotted line in the figure indicated the crack.

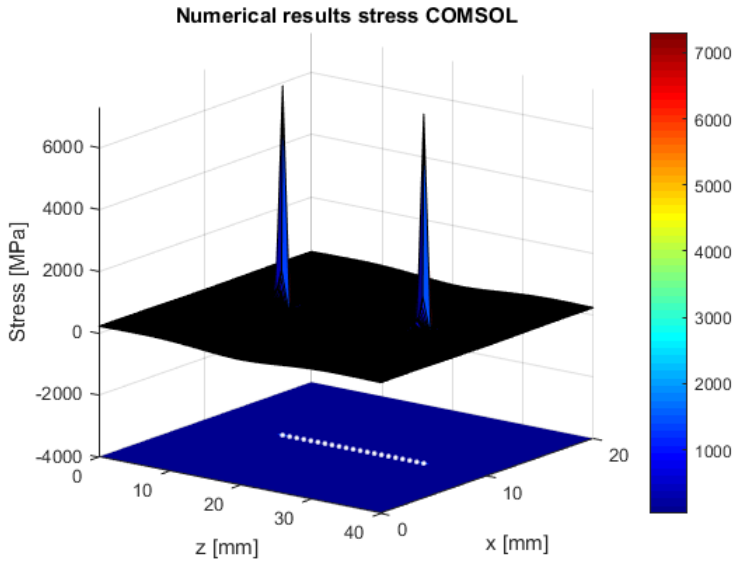

Figure 5.4: Numerical results for the stress distribution around the fatigue crack

5.4. Magnetic FEM model - stress-induced magnetization

This FEM model shows the induced magnetism for the steel plate since the permanent magnetization and the stress-induced magnetization cannot be modeled in COMSOL Multiphysics.

Geometry

The geometry is modeled in COMSOL Multiphysiccs as shown in 3.8 with a box of air around it of 15 x 15 x 15 m (L x B x H). The geometry of the defect causing the stress concentration is also shown in this figure. The results were obtained for the area around the defect that is covered by the grid in figure 3.9.

Materials & Meshing

The same materials & meshing were applied as in section 5.2.

Boundary conditions

The same boundary conditions were applied as in section 5.2.

Results

The magnetic flux density in y-direction is calculated for the entire area around the stress concentration as shown in figure 5.5.

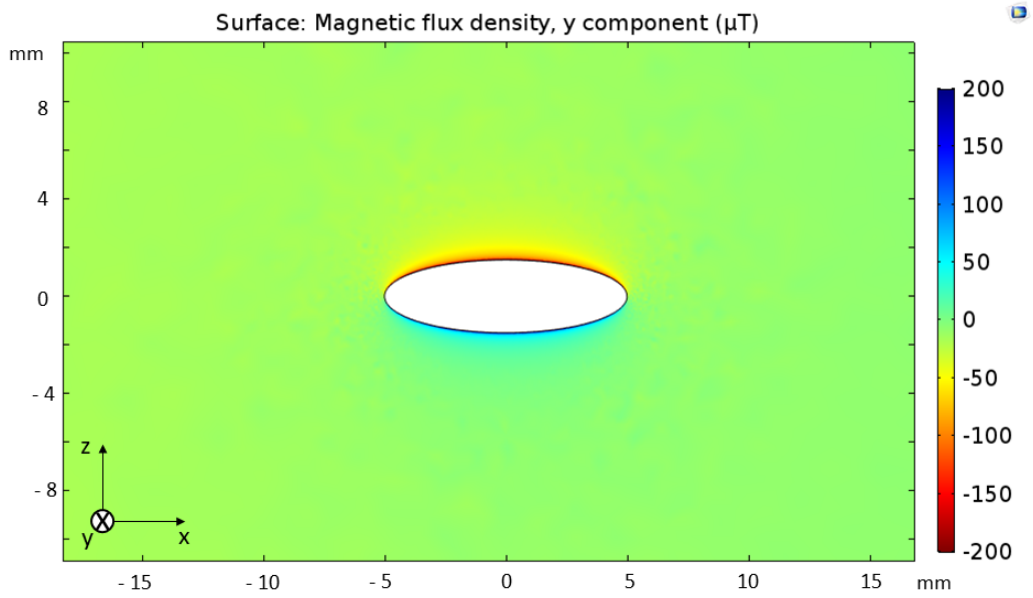

Figure 5.5: Numerical results B_y stress concentration

5.5. Stress model - stress-induced magnetization

To indicate the distribution of stresses around the stress concentration a FEM model was build. In this model the Von Mises stresses are calculated for the plate being in tension at a nominal stress level of 235 MPa. Also, this model is used to calculate the stresses 50 mm above the stress concentration for a maximum nominal stress level of 220 MPa. This is used for the follow-up experiment.

Geometry

The geometry as well as the defect is modeled in COMSOL Multiphysiccs as shown in 3.8. The results were obtained for the entire area that is covered by the grid in figure 3.9 around the defect.

Materials & Meshing

The same materials & meshing was applied as in section 5.3.

Boundary conditions

The same boundary conditions were applied as in section 5.3. The only difference for this case is the condition 'Boundary Load' which is set at a force per unit area of $235 \cdot 10^6$ N/m^2. This force is set in positive z-direction for the top boundary of the plate. For the follow-up experiment this was set to $220 \cdot 10^6$ N/m^2.

Results

The Von Mises stresses are calculated for the entire area around the stress concentration as shown in figure 5.6.

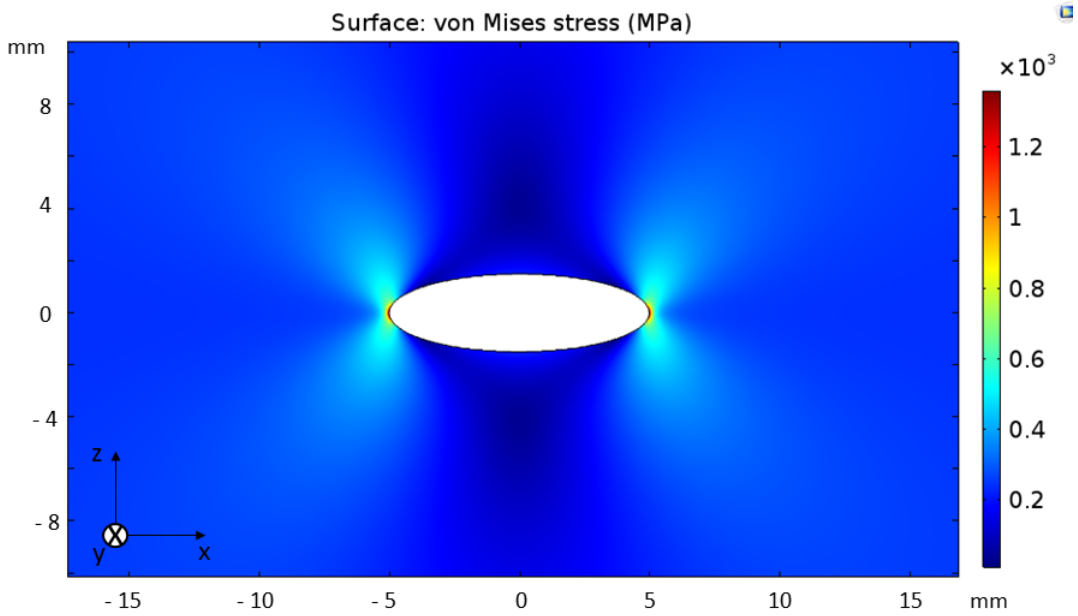

Figure 5.6: Numerical results for the stress distribution around the stress concentration

For the follow-up experiment the Von Mises stresses are calculated for the entire area around the stress concentration as well as the area 50 mm above it. This is shown in figure 5.7.

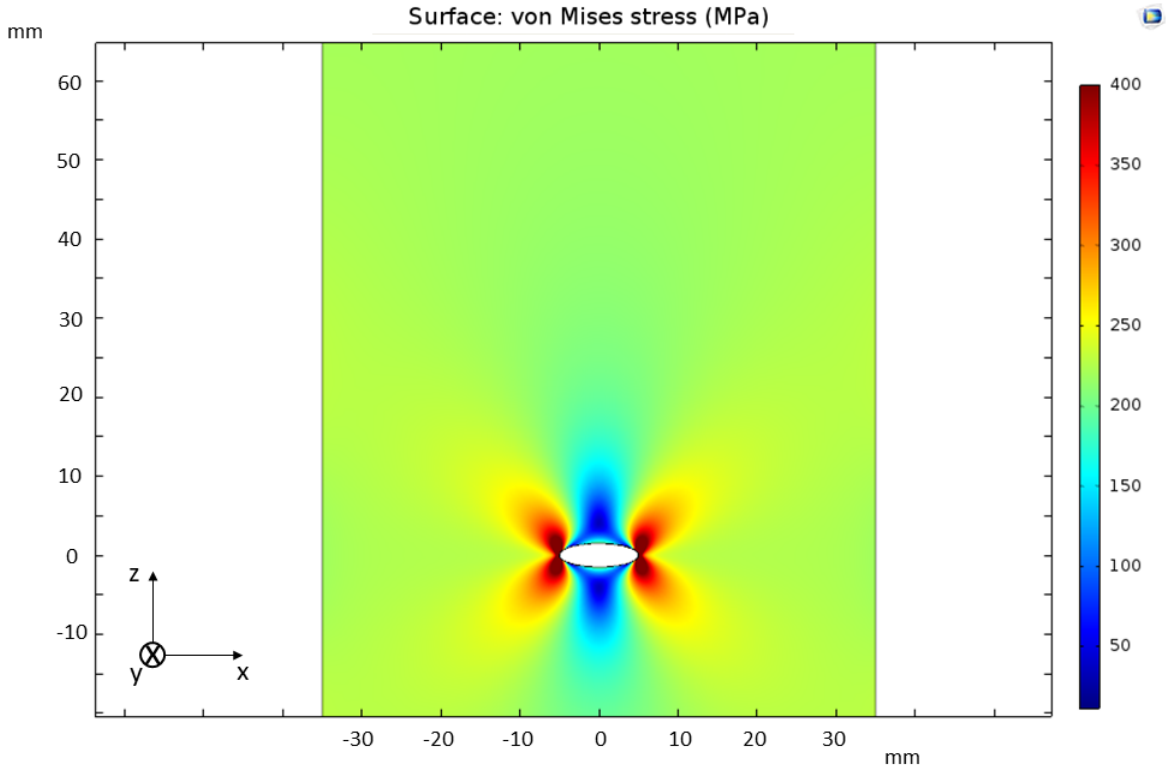

Figure 5.7: Numerical results for the stress distribution around the stress concentration

5.6. The effective field description

The effective field description described in section 2.2.3 can numerically be solved with the Euler forward method. This is done by PhD student Aad Vijn from the faculty of Applied Mathematics at the Delft University of Technology with the following numerical scheme implemented in Matlab. To insure stability the applied stress signal should not vary fast.

$$M_{n+1} = M_n + (\sigma_{n+1} - \sigma_n) F(\sigma_n, M_n) \tag{5.1}$$

where F is equation 2.41

$$F(\sigma_n, M_n) = \frac{dM}{d\sigma} = -\frac{(M - M_a - ck\delta \frac{dM_a}{dH_e})(B_1 M + B_2 M\sigma)}{k\delta + (M - M_a - ck\delta \frac{dM_a}{dH_e})(\alpha + B_1\sigma + \frac{1}{4}B_2\sigma^2)}$$

and

$$\sigma_{n+1} = \sigma(t_{n+1})$$

and

$$\sigma_n = \sigma(t_n)$$

and

$$M_0 = M|_{\sigma=\sigma_0, H=H_a}$$

The results of the model describing the effective field description are obtained with the parameters in table 2.2 and an applied field according to the measured background field in table 3.2. The initial magnitization is chosen arbitrarily as 30 % of the saturation magnetization. The results are presented in figure 5.8.

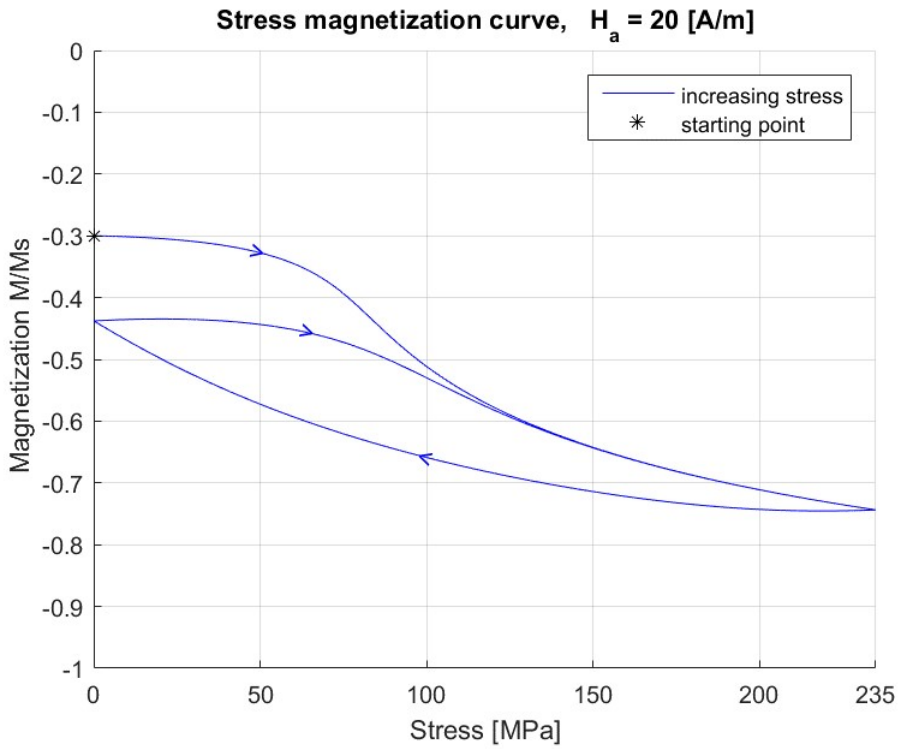

Figure 5.8: Model results for the effective field description

5.6.1. The effective field description - Compression

To give an indication of the behavior of the stress magnetization curve under compression figure 5.8 is extended. This is done by extending the force-time diagram (figure 3.7) with a negative force up to -82.25 kN as shown in figure 5.9. The model results are presented in figure

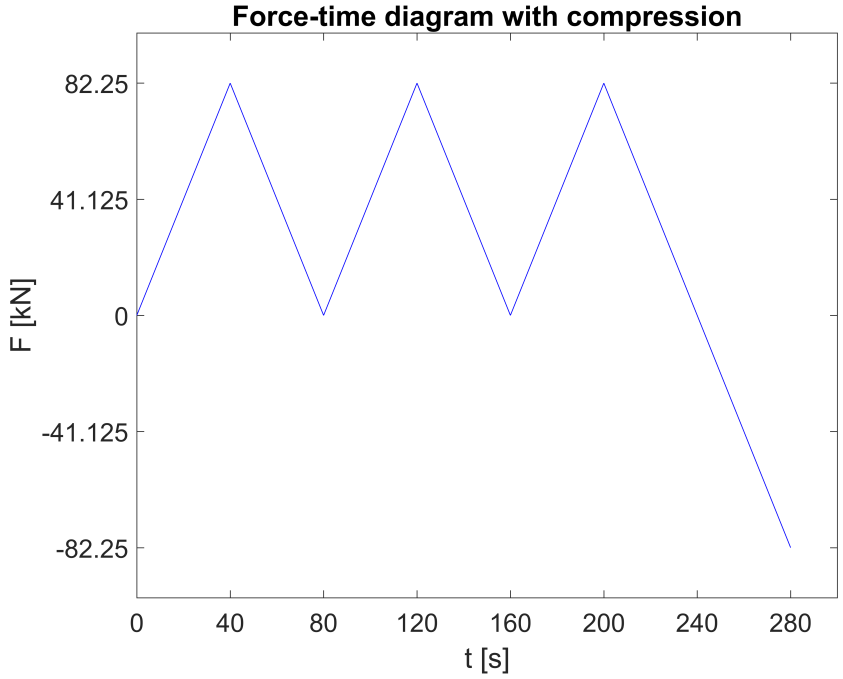

Figure 5.9: Extended force-time diagram for compression force

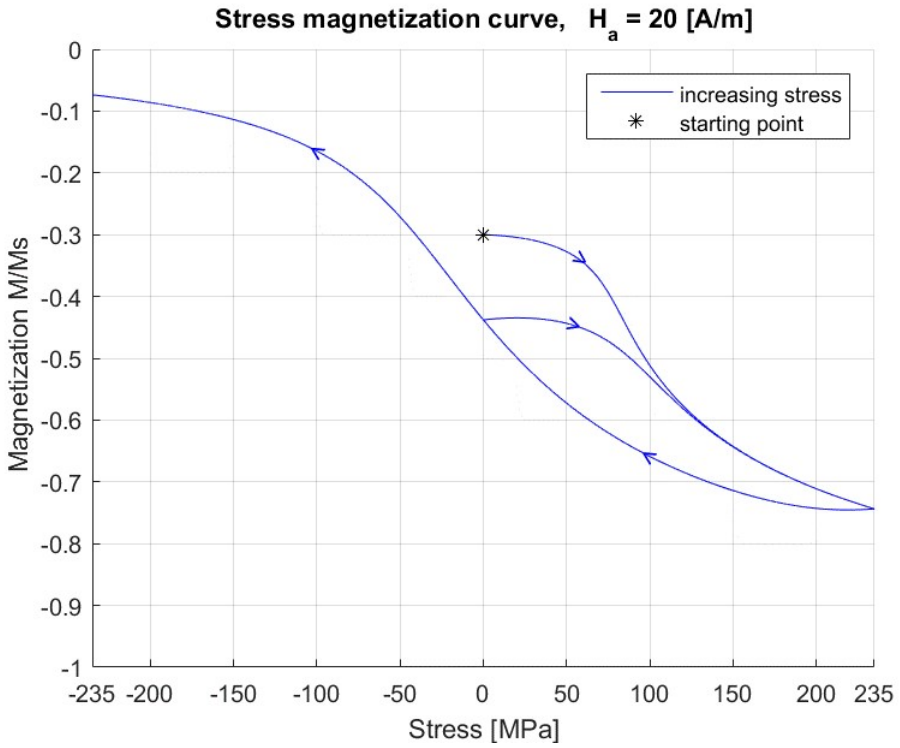

Figure 5.10: Model results extended with compression

6

Conclusions

In this chapter, the conclusions of this research are presented based on the results of the experiments. The experimental results are also compared to the findings from literature and numerical simulations. Each research question will be answered in a separate section.

Is it possible to detect a fatigue crack in a steel plate that is in tension with a Hall sensor measuring the magnetic flux density?

The results of the magnetic flux density signal for an open crack is shown in figures 4.1, 4.2 and 4.3 in section 4.2. They show that the magnetic flux density keeps increasing for a propagating crack in the vicinity of the crack. This is in line with the literature described in section 2.2.3. When the crack opening is increased, the SMFL increases, resulting in a higher signal of the magnetic flux density. An interesting result is that from cycle 719292, the crack grew into a through thickness crack and the magnetic flux density suddenly increased when cycle 729378 was reached. This is clearly illustrated in figures 4.6, 4.7 and 4.8, where the magnetic flux density increases for every millimeter of crack propagation. The difference between cycles 729378-719292 shows a sudden increase of 8 μT in the vicinity of the crack. This can be explained by the occurrence of an air gap resulting in a sudden increase in the SMFL. After that moment, the change in magnetic flux density only increases slightly since the crack has already opened and the only increase comes from the crack becoming longer. This is not a sudden increase but more gradual as can be seen in the figures 4.7 and 4.8.

In figures 4.9, 4.10 and 4.11, the differences between the results for an open crack and a closed crack are presented. These figures give clear insight into the increase of SMFL due to the opening of the crack. Especially near the crack tips, this difference is significant, which could give an indication of the location and length of the crack. The signal increase due to crack opening corresponds to the theory but to accurately determine the length of the crack, it is important to know if the signal behaves as described in literature. This will be explained in the next question.

The magnetic flux density signal for the closed crack is presented in figures 4.4 and 4.5. They show an increase in B_y in the vicinity of the crack during crack propagation. This result is not in accordance with the expectations because, theoretically there is no air gap that can increase the signal of the magnetic flux density. When the crack is closed, the magnetic flux is not able to 'leak' into the air. The increase in B_y is probably since the fatigue machine still applied a tension of 3 kN at its minimum, causing a small crack opening.

It concludes that it is possible to detect a change in magnetic flux density in the vicinity of the fatigue crack for a steel plate under tension. It can potentially indicate the location of the crack. Monitoring the crack would be possible if there is more knowledge of the occurrence of these peaks at the crack tips. In the next question the resemblance between the classic SMFL signal in the vicinity of a crack and a crack in tension will be discussed.

Does the magnetic flux density signal for a fatigue crack brought into tension behave the same as for cracks that are not?

To investigate the expected magnetic flux density signal of the same plate as described in section 3.2 a numerical model was made in section 5.2. The fatigue crack is modeled in open position but the permanent

magnetism and the stress-induced magnetism are not modeled because this is not possible in COMSOL Multiphysics.

The result in figure 5.2 is compared to the results of an open crack which is shown in the last picture of figure 4.3. The numerical results show that the signal has a negative half peak on the left side of the crack and positive half peak on the right side. This is in accordance with the experimental results of Van der Horst [27] and the theory described in section 2.2.3 for plates which are not in tension. The behavior of the magnetic flux density of the experimental results differs from the modeled results. The FEM model shows that the signal has a negative half peak on the left side of the crack and positive half peak on the right side. However, the results of the experiment show that two peaks occur at the crack tips (figure 4.3).

This phenomenon could be due to stress-induced magnetization which is described in section 2.2.3. To investigate this, a mechanical FE model was built, see figure 5.4. The model can indicate where the highest stresses occur in the plate and this shows the location where the stress-induced magnetization effect probably has the highest contribution. Figure 5.4 shows the highest stresses at the crack tips. This is also expected since a stress concentration will occur at the crack tips.

This could mean that the SMFL due to the opening of the crack is smaller than the effect of the high stresses at the end of the crack. This could be an explanation for the peaks occurring at the crack tips as shown in figure 4.3. This is likely due to the stress-induced magnetization which has the highest contribution at the crack tips and the smallest contribution in the middle of the crack.

It is concluded that the signal shows a different behavior when the steel plate is brought into tension compared to a plate which is unloaded. Therefore, further research is needed to be able to determine if the peaks are due to the concentrated stresses at a crack tip. That way the crack length could be monitored even though the crack opening effect is dominated by the stress-induced magnetization.

Is the effect of the stress-induced magnetization significant on the magnetic flux density signal of a steel plate with a fatigue crack?

The experiment described in section 3.3 was conducted to answer this question. In this experiment, the SMFL due to the change of the opening of the crack is minimized by choosing an elliptical hole as defect as explained in section 3.3.1. This resulted in the stresses being concentrated at the tips of the elliptical hole as shown in figure 5.6.

The raw data in figures 4.12, 4.13 and 4.14 show the total measured magnetic flux density. A periodic behavior can be noticed from these results. To look solely into the contribution of the stress-induced magnetization, figures 4.15, 4.16 and 4.17 need to be considered. The results show a periodic change of the stress-induced magnetic flux density, which corresponds to the period of the applied tension as shown in figure 3.7.

Figures 4.15, 4.16 and 4.17 show the range of the contribution of the stress-induced magnetization for a steel plate with a geometry as in figure 3.6. This contribution differs from 8 μT for point (3,1) up to a contribution of 25 μT for point (1,2). The amplitudes for points (1,1) and (1,2) are very high which correspond with the locations of occurrence of higher stresses (figure 5.4). Point (1,3) is at the neutral line where the stresses are very low according to the numerical results. This is more clearly illustrated in figure 4.24 where the hysteretic curves for point (1,2) and (1,3) are plotted. The high stresses occur at point (1,2) while point (1,3) is located at the neutral line.

It is expected according to FEM model in figure 5.5 that the stress-induced magnetization is symmetric like the stresses. In figure 4.19 the symmetric points (1,1), (1,5), (3,1) and (3,5) are plotted. However, they are not symmetric. The same applies if row 1 and row 3 are compared which should be symmetric as well. This is likely due to inhomogeneous distribution of the permanent magnetism in the material which is assumed constant under varying stress.

Figures 4.15, 4.16 and 4.17 show that at the start of every new cycle a small downward peak can be observed. This is probably due the overshoot of the MTS machine inducing bending stresses into the specimen. Since the specimen is very slender a small compression force can result in relatively large bending stresses in

the specimen. This clearly illustrated in the curve of grid point (1,3) in figure 4.22. This grid point is located at the neutral line where the stresses theoretically not increase. The contribution at this point is about 0 μT except for the beginning of the curve. The magnetic flux density increases only at the start of the graph probably due to the induced bending stresses.

It is concluded that the stress-induced magnetization can have a significant contribution on the SMFL in areas where the stresses are concentrated. A fatigue crack has an open position when the crack is under tension or in bending, meaning that the opening effects described in section 2.2.3 can be dominated by stress-induced magnetization. This depends on geometry of the structure, the geometry of the crack, the magnetization, the magnetostriction and the stresses that are exerted on the structure. Since, stress concentrations occur at the crack tips for fatigue cracks, as shown in figure 5.4, it is essential to take this into consideration for monitoring fatigue cracks. If the results would be assessed with only the knowledge of the SMFL due to crack opening, the crack size cannot be accurately determined and a wrong course of action could be taken. This could result in premature failure of the steel structure or unnecessary repair.

Does the effect of the stress-induced magnetization on the magnetic flux density signal of a steel plate with a crack correspond to the behavior described in the literature?

The effective field description results are found in figure 5.8. In this model, the magnetization initially decreases after which it stays in the same hysteretic curve. This can be explained as the hysteretic curve approaching the anhysteretic curve. The initial decrease is the first stress cycle applied on the material. This can be neglected when comparing the results because this stress is applied before the measurements presented in the results were obtained.

Figures 4.21, 4.22 and 4.23 show the average of the 3 periods that the force is increasing and decreasing. These results can be compared to the simulation results from the effective field description. Absolute values cannot be compared because this model does not take the permanent magnetism into account. The results show a hysteretic behavior with a similar curve obtained in the effective field description shown in figure 5.8.

Some of the hysteretic curves in figures 4.21, 4.22 and 4.23 do not close at a force of 0 kN. This could be explained by the fact that the MTS machine gave an overshoot which exerted compression forces on the plate causing a different signal.

To investigate the long-term effects of cyclic loading, the experiment is repeated for 24 cycles for point (1,2) after the entire grid was measured. The raw data are plotted in figure 4.25. Three cycles at the start of this measurement are compared with three cycles at the end. The previous measurement of point (1,2) was also compared. These three curves are shown in figure 4.26. The measurements done after repeating the cycles (orange curve) have a smaller amplitude than the previous measurement (blue curve). At the end of the 24 cycles (yellow curve), the amplitude is again slightly smaller than at the beginning of this measurement (orange curve). This could indicate that the magnetic signal approaches anhysteretic magnetization since the extra cycles could cause a part of the magnetization to be demagnetized, resulting in a smaller amplitude of the stress-induced magnetization.

It is concluded that the experimental results behave in a hysteretic manner, which is in correspondence with the literature describing the effective field description. Also, the results seem to indicate that the magnetization approaches the shape of the anhysteretic magnetization since the results show a decreased signal after applying several stress cycles.

What is the difference between the magnetic flux density signal of a plastically deformed part of the steel plate and the elastically deformed part?

Figure 5.7 shows that there is no effect of the stress concentration 50 mm above the middle of the elliptical hole. The stress at the location of row 0 is 220 MPa for every grid point. This resulted in the hysteresis curves of row 0 presented in figure 4.30. The hysteretic behavior is still observed for all the results which is in accordance with the effective field description. These show a range of 10 μT to 19 μT. The range for the stress-induced magnetization is expected to be the same for every grid point of row 0 because the maximum stress also remains the same for every grid point. This is the case for every point on row 0 except for point (0,1), where the range is 19 μT instead of 10 μT for the other points. This difference may be explained by the

permanent magnetism in the steel plate, which is different for every location. The permanent magnetism is coupled with the stress-induced magnetization. This range is smaller than the range found in the results of the hysteretic curves around the stress concentration. This can be due to the stress range being larger around the stress concentration compared to the area that is not affected by it.

It concludes that plastic deformation has no significant effect on the behavior of the stress-induced magnetization, since the same hysteretic behavior is observed. The range of the contribution of the stress-induced magnetization depends on the range of stresses that is reached at a specification location. Also, local differences occur probably due to inhomogeneous distribution of the permanent magnetization in the material.

What effect does the stress-induced magnetization have on crack monitoring by self magnetic flux leakage on a steel plate?
The stress-induced magnetization causes the magnetic flux density to increase at the location where the stresses are concentrated. These stress concentrations occur at the crack tips of a fatigue crack. This effect can be dominant against the crack opening effect depending on the geometry of the structure, the geometry of the defect, the magnetization, the magnetostriction and the applied stress. This causes the signal to increase at the crack tips and not show the classic negative and positive half peak across the length of the crack. In this research, the range of the contribution of the stress-induced magnetization for a steel plate with the geometry presented in figure 3.6 is experimentally determined. The range around the stress concentration is between 8 μT and 25 μT. For the region on the plate where the defect has no effect anymore the range is between 10 μT and 19 μT.

The experiment with a through thickness crack described in section 3.2 has a peak-to-peak value of B_y of 22 μT as can be seen in the last picture of figure 4.3. This means that the contribution of the stress-induced magnetization is between 36 % and 113 % according to the results for the experiment in section 3.3. This is under the assumption that the stresses would be the same for the plate with the fatigue crack and the plate for determining the range of stress-induced magnetization. This is not the case as can be seen in the results of the stress models made in COMSOL Multiphysics in figures 5.6 and 5.4. It can be seen that the maximum stress for the fatigue crack at the crack tip is 5 times higher than the maximum stress of the elliptical defect. This would result in an even higher contribution of stress-induced magnetization. It needs to be taken into account that the permanent magnetization is not homogeneous which could result in locally different contributions. Concluding, the stress-induced magnetization dominates the crack opening effect in the experimental case presented. Therefore, the stress-induced magnetization should be taken into account for the interpretation of the magnetic flux density to determine the crack size.

Steel plates used in the offshore and maritime industry are usually thicker than 5 mm in which the fatigue cracks occur. At the department of Civil Engineering of Delft University of Technology, a steel bridge deck is being tested in fatigue. In this deck, a 30 mm long fatigue crack is induced in a steel plate with a thickness of 20 mm. The peak-to-peak value measured over the crack is approximately 800 μT. The contribution of the stress-induced magnetization according to the range determined in this research is between the 1 % and 3 %. The contribution could be higher in reality if the stresses at the crack tip are higher than the stresses around the elliptical hole. Still, the measured results of the crack in the bridge deck shows the expected SMFL signal by the crack opening effect of a fatigue crack. This could have been expected since there is more material that can be magnetized, resulting in a higher magnetic flux leakage. Monitoring this fatigue crack using the SMFL can be done without any corrections for the stress-induced magnetization.

Monitoring elliptical fatigue cracks that have not fully grown through the thickness of the plate would be a useful addition for the offshore and maritime industry. Numerical models for elliptical defects with different geometries are made by ROSEN group. In these models, the permanent magnetism is not taken into account. The calculated range of the peak-to-peak value of the magnetic flux density is between 2 μT and 32 μT. The contribution of the stress-induced magnetization is between 400 % and 1250 % for the lower case and between 25 % and 78 % for the upper case. This is also under the assumption that the stresses in the elliptical defects are the same as for the stress concentration in figure 5.6. This contribution is significant concluding that for monitoring elliptical fatigue cracks measuring the SMFL a correction is needed for the stress-induced magnetization.

This research concludes that the stress-induced magnetization can have a significant effect on monitoring the length of a fatigue crack using the SMFL method. Its significance depends on the geometry of the structure, the geometry of the crack, the magnetization, the magnetostriction and the stresses that are exerted on the structure. The signal caused by the stress-induced magnetization can dominate the SMFL that occurs due to the crack opening effect. To accurately determine the length of a fatigue crack using the SMFL method, it is necessary to further investigate the contribution of the stress-induced magnetization. With this knowledge, a correct decision can be made on what course of action should be taken to maintain the integrity of the structure.

7

Discussion

This chapter reflects on the results found during experimental testing and modeling. Recommendations for further research and application are also done in this chapter.

Measurement errors

Three experiments were carried out in this thesis and steps were taken to increase the quality of the results. Errors can occur while measuring the magnetic flux density such as the varying distance between the plate and Hall sensor. If this distance increases the measured magnetic flux density will decrease rapidly. In this research, this was ensured by a plastic tube around the Hall sensor that sticks out 1 mm in front of it. It is also essential that the probe is exactly perpendicular to the steel plate to measure strictly in one direction along the chosen axis. The plastic tube around the probe helps to achieve this since it has a bigger surface than the probe that can be put on the plate.

During the measurements of the experiment described in section 3.3, the probe was held on the same location for 4 minutes by hand. Since the permanent magnetism is not distributed homogeneously through the material it is important that the probe is held on the same position on the plate while doing a measurement. This was insured by drawing a grid on the steel plate. For the induced magnetism modeled in figure 5.5, the sensitivity for the placement of the sensor is low because the plate adapts to the value of the induced field in y-direction of table 3.2 except for the edge of the elliptical hole.

During this experiment the MTS machine and the measurement of the Hall sensor were manually simultaneously started and stopped. The internal clock of the program for the Hall sensor did also not measure exactly every 0.2 s. It differed between 0.17 and 0.22 s. This resulted in the amount of measurements not exactly corresponding to the expected 1200 measurements. While processing the data the peaks of every cycle where determined to indicate when a new stress cycle started. This could have been more accurate if the MTS machine did not overshoot and no bending stresses were introduced into the specimen. A solution for that is to set the MTS machine not to approach a force of 0 kN but for example of 3 kN, which was done for the follow-up experiment described in section 3.4.

Permanent magnetism

The two components that determine the self magnetic flux leakage are the induced magnetism and the permanent magnetism. The permanent component is hysteretic and inhomogeneous distributed in the material. For that reason, it is not possible to model this in a FEM model. This causes always a discrepancy between the numerical and experimental results. Still, the numerical results can give more insight in the experimental results since it represents the distribution of the induced magnetism.

In this research it is assumed that the total stress-induced magnetization can be uncoupled from the permanent magnetization (equation 2.2) but this is incorrect since the irreversible part of stress-induced magnetization is part of the permanent magnetization. Still, equation 4.1 can be applied for determining the

stress-induced magnetization, since there are no irreversible effects visible in the stress-induced magnetization curves. The reversible magnetization becomes more dominant after more applied stress cycles because the anhysteretic magnetization is approached as explained in section 2.2.3.

The stress-induced magnetization is dependent on the total magnetization which entails the permanent magnetization of the material. Therefore, local differences in the range of the stress-induced magnetizations can be observed. This is shown in figure 4.19, where points (1,1), (1,5), (3,1) and (3,5) are plotted. These four points should show the same amplitude for the stress magnetization in the results due to the symmetry of stresses at these points. This is not the case and could indicate that the permanent magnetism cannot be decoupled from the stress-induced magnetism. Still, the contribution of the stress-induced magnetization is generally bigger in areas were the stresses are higher and smaller where the stresses are lower. This difference is shown in figure 4.24 as explained in chapter 6.

For measuring only, the stress-induced magnetism the steel plates could have been demagnetized before the experiment but this might also have effect on the amplitude of the stress-induced magnetization. It would be interesting for future research to use exactly the same plates and demagnetize before loading them again. From these results the effect solely of the stress-induced magnetization could be determined.

Effective field description

In the effective field description, it is assumed that the direction of the induced field H_a has the same direction as the direction in which the stress is applied. Since the specimen is not actively magnetized the only field that acts on it is the Earth magnetic field. The angle between the Earth's magnetic field and the direction of the applied stress needs to be determined and added to the stress component of the effective field description which is presented in equation 2.10. This angle can be added with the Poisson ratio as described in equation 2.3 [18]. The added part to the equation described below is colored red to indicate how the factor of the angle can be added to the effective field description.

$$H_\sigma = \frac{3}{2}\frac{\sigma}{\mu_0}\frac{d\lambda}{dM}(cos^2\theta - vsin^2\theta) \tag{7.1}$$

Another factor that is important to consider in this model is α which is the dimensionless parameter representing interdomain coupling. This parameter is determined for the exact middle of an ellipsoid made from steel. When the location is slightly changed within the ellipsoid this parameter already changes. Since the measurements are taken 1 mm outside of the plate the parameter α would have a different value. Further research is needed to be able to determine this parameter outside the material. This results in a discrepancy between the effective field description and the experimental results.

Application

The SMFL method is used in a sensor for monitoring through thickness fatigue cracks in large steel structures and is called the CrackGuard sensor. In Appendix B the components of the sensor are explained in more detail and an experiment is conducted with the actual CrackGuard sensor.

An useful addition would be if the CrackGuard could be applied for elliptical fatigue cracks that are not fully propagated through the thickness plate as already suggested in chapter 6. To achieve this the phenomena of stress-induced magnetization needs to be better understood to accurately link the signal of the magnetic flux density to a crack length, since elliptical fatigue cracks give a lower signal compared to through thickness cracks. This results in the stress-induced magnetization having a significant contribution to the measured signal. With this addition the CrackGuard sensor could have a wider application for monitoring fatigue cracks. Also, a more accurate decision can be made what course of action should be taken to maintain the integrity of the structure.

Future research

This research has shown that the stress-induced magnetization has effect on measuring the crack length using the SMFL method when a steel plate is in tension. This effect needs to be further researched to accurately determine the crack length in tension or compression because fatigue cracks are usually opened when stress is applied on the material. Understanding the stress-induced magnetization makes it possible to more accurately determine the crack length and decide on the course of action that needs to be taken.

This research only considered stresses that occur due to tension in the material, but stresses can also occur due to compression. The effective field model is extended in section 5.6.1 with a compression force after three cycles in tension. The result in figure 5.10 shows that the behavior is different in compression, indicating that the behavior is anti-symmetric. This should be further researched with experiments. This would mean that the contribution of the stress-induced magnetization can have twice the range found in this research. Resulting in that the contribution of stress-induced magnetization can be significant depending on the application and that further research in to this will be a valuable contribution for the application of the SMFL method.

The thickness of the steel plates used in the offshore and maritime industry are normally thicker than 5 mm and the volume of material is much larger. This extra volume of steel can be magnetized by the Earth's magnetic field and causes an increase of magnetic flux density even though the stresses in the material stay the same. This could result in the effect of stress-induced magnetization being dominated by the crack opening effect. This could be investigated by repeating the experiment described in section 3.3 with plates with bigger thicknesses like 10, 15 and 20 mm and applying a tensile load up to the yield strength for every plate. If the result would resemble the behavior of the numerical results presented in figure 5.5, it could be caused by the fact that the stress-induced magnetization is not dominant compared to the crack opening effect.

Based on the results of the long-term effects of cyclic loading (section 4.3.4), it seems that the anhysteretic magnetization curve is approached after a certain amount of stress cycles. This is interesting for the application of the CrackGuard sensor because it monitors fatigue cracks that occur after multiple cycles. This can contribute to correctly assessing the data if it is known when the anhysteretic magnetization is approached because this behavior predictable. It would give the opportunity to predict the signal that would occur due to the stress-induced magnetization.

Fatigue cracks are not only induced by cycles with the same stress range. This depends among other things on the wave spectrum in maritime and offshore structures. It would be interesting to investigate if even though the stress cycles are not the same, still the same anhysteretic curve is approached. This could be done by inducing a spectrum of stress cycles that are similar to real life wave conditions and investigate if the same anhysteretic magnetization will be found by inducing the same stress cycle.

A

Experiment fatigue crack

A.1. Parameters fatigue test

To insure that a fatigue crack will initiate at the location of the defect the following calculation is made. The delta load used in this fatigue test is 81 kN. This results in a delta stress at the defect of

$$\Delta\sigma = \frac{\Delta F}{W \cdot \frac{W}{W_{grip}} \cdot t} \tag{A.1}$$

with W being the width of the plate (90 mm), W_{grip} (75 mm) the width over which the plate is clamped and t the thickness (5 mm). The factor $\frac{W}{W_{grip}}$ is implemented since the gripping is smaller than the width of the plate resulting in a lower stress over the width of the plate.

For this case the ΔK is calculated at the deepest point of the defect according to equation 2.46. This point is for $\theta = \frac{\pi}{2}$ this results in

$$8.23 \quad \text{MPa}\sqrt{m} > 6.4 \quad \text{MPa}\sqrt{m} \tag{A.2}$$

since the threshold is exceeded a fatigue crack will initiate at the location of the defect.

B

Experiment CrackGuard sensor

B.1. Introduction

In this appendix an experiment is done with the CrackGuard sensor. This sensor makes use of the SMFL method to monitor fatigue cracks as mentioned in chapter 7. The CrackGuard sensor consist of 60 Hall effect sensors, which measures the voltage difference that occurs when a magnetic field is applied to a ferromagnetic material[24]. Also, the sensor contains a backplane. This backplane is made of steel and ensures that the signal will be picked up by the sensors by spreading the signal more widely. The disadvantage of this is that the signal strength is lowered.

In this experiment it is investigated if the CrackGuard sensor can monitor a fatigue crack in a plate brought into tension. Also, a numerically study is done to investigate the effect of different backplanes.

B.2. Experimental testing

B.2.1. Geometry

For this experiment a 5 mm thick plate is used with the dimensions presented in figure B.1. It is made out of steel with a yield strength of 235 MPa. The dimensions of the defect in the plate are the same as in figure 3.2.

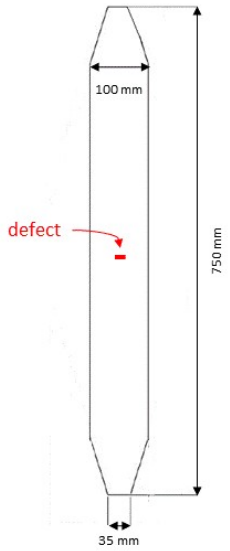

Figure B.1: Geometry plate for experiment CrackGuard sensor

B.2.2. Experimental setup

In this experiment the CrackGuard sensor is used, which consist of 60 Hall effect sensors positioned in a grid as shown in figure B.2. In every row the sensors are spaced 11 mm between each other and every next row is shifted by 5.5 mm. The distance between the rows is 11 mm. The sensor also includes a battery pack which functions as the power source of the sensor and all of this is poured into a mold of flexible plastic. On top of the sensors the backplane is placed to insure that the signal of the crack is picked up by one of the Hall sensors.

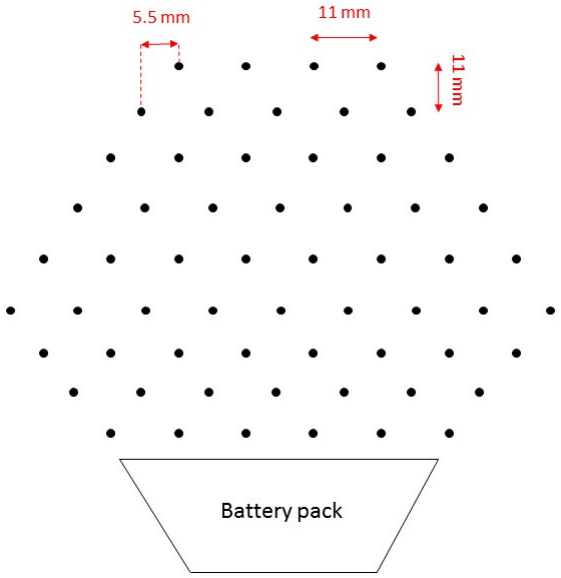

Figure B.2: Schematic CrackGuard sensor

Figure B.3 shows the experimental setup. The specimen is axial loaded in a MTS fatigue testing machine that has a maximum range of -350 kN to 350 kN, to induce a fatigue crack in the specimen. The CrackGuard sensor is placed over the defect as shown in figure B.3. It will measure the magnetic flux leakage out of plane. The fatigue crack will propagate in the direction along the x-axis, this corresponds to the crack propagating in the direction of the width of the specimen. The x, y and z axis are chosen accordingly to figure B.3.

Figure B.3: Experimental setup experiment CrackGuard sensor

The background field that was measured for this experiment is presented in table B.1. This is measured in the area where the experiment takes place.

Axis background field	Magnetic flux [μT]
x	8
y	16
z	-31

Table B.1: Background field experiment CrackGuard sensor

B.2.3. Parameters fatigue test

The same parameters as appendix A are used for this experiment. For this case the delta stress is calculated according to equation A.1 but for a width of $W = 100$ mm. This results in a δK of

$$6.70 \quad \text{MPa}\sqrt{m} > 6.4 \quad \text{MPa}\sqrt{m} \tag{B.1}$$

since the threshold is exceeded a fatigue crack will initiate at the location of the defect.

B.3. Experimental Results

The results magnetic flux density measured with the CrackGuard sensor are presented in figure B.4. The black line gives an indication of the crack length on the opposite side of the plate.

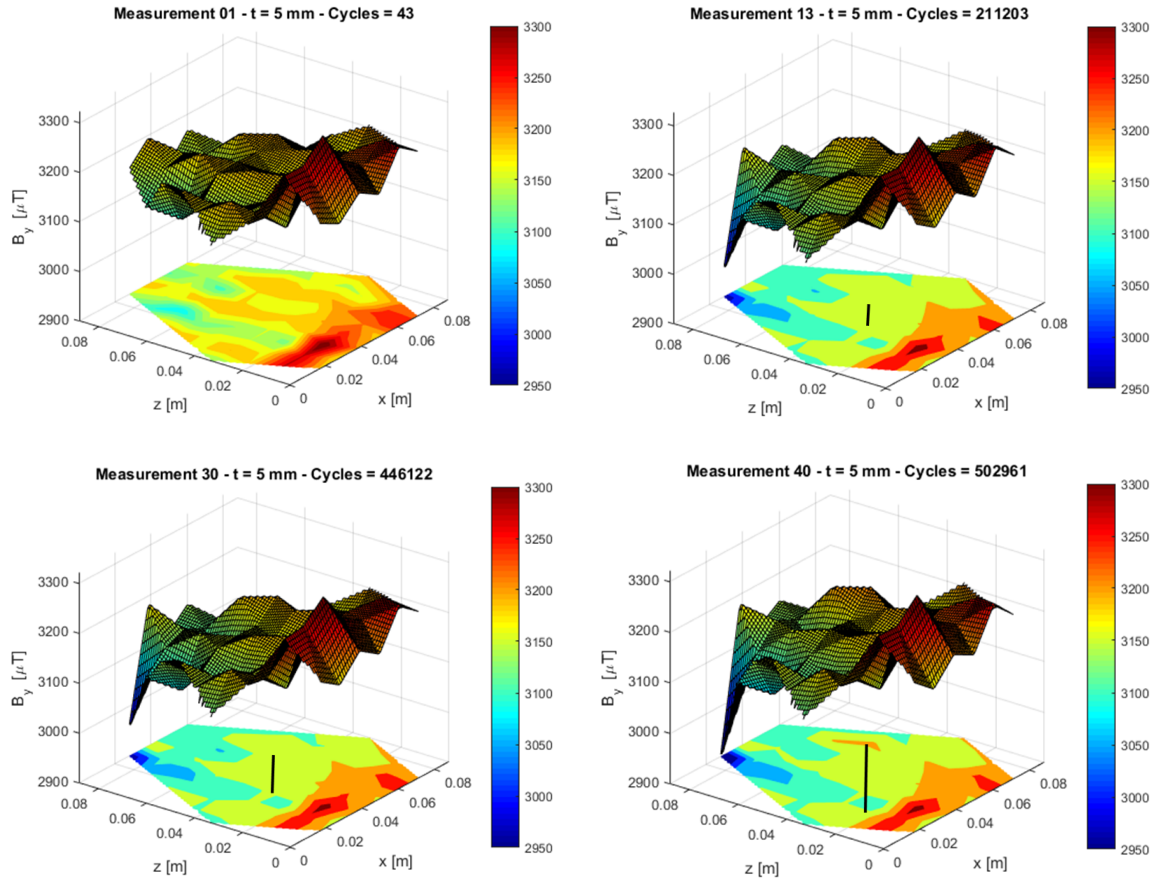

Figure B.4: B_y for the measurements with CrackGuard sensor

From these results it can be seen that there are only small changes and there is no signal that indicates the crack properly. Under these conditions the CrackGuard sensor is not accurate enough to monitor a fatigue crack. To be able to monitors this fatigue crack more sensitive Hall sensors are needed.

B.4. Numerical Simulation

In this experiment the backplane can influence the magnetic flux density measured by the CrackGuard sensor since the backplane lowers the signal. The effect of three different back planes is modeled, without a back plane, with a solid back plane and the CrackGuard sensor back plane to see how this effects the SMFL.

Geometry

The geometry is modeled in COMSOL as shown in B.1 with a box of air around it of 15 x 15 x 15 m (L x B x H). The geometry of the defect is modeled as an through thickness crack with a width of 60 mm and an opening of 2 mm as shown in figure B.5. Three different options for back planes where modeled: without a back plane, with a solid back plane and the last with the geometry of the CrackGuard back plane. Between the specimen and the back plane an air gap of 1 mm is modeled. The geometry of these are presented in figure B.6.

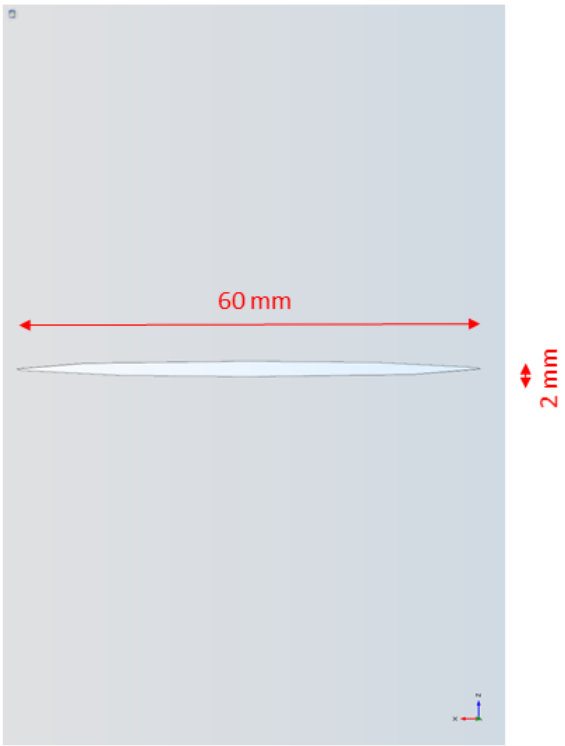

Figure B.5: Dimensions of the defect modeled in a FEM model

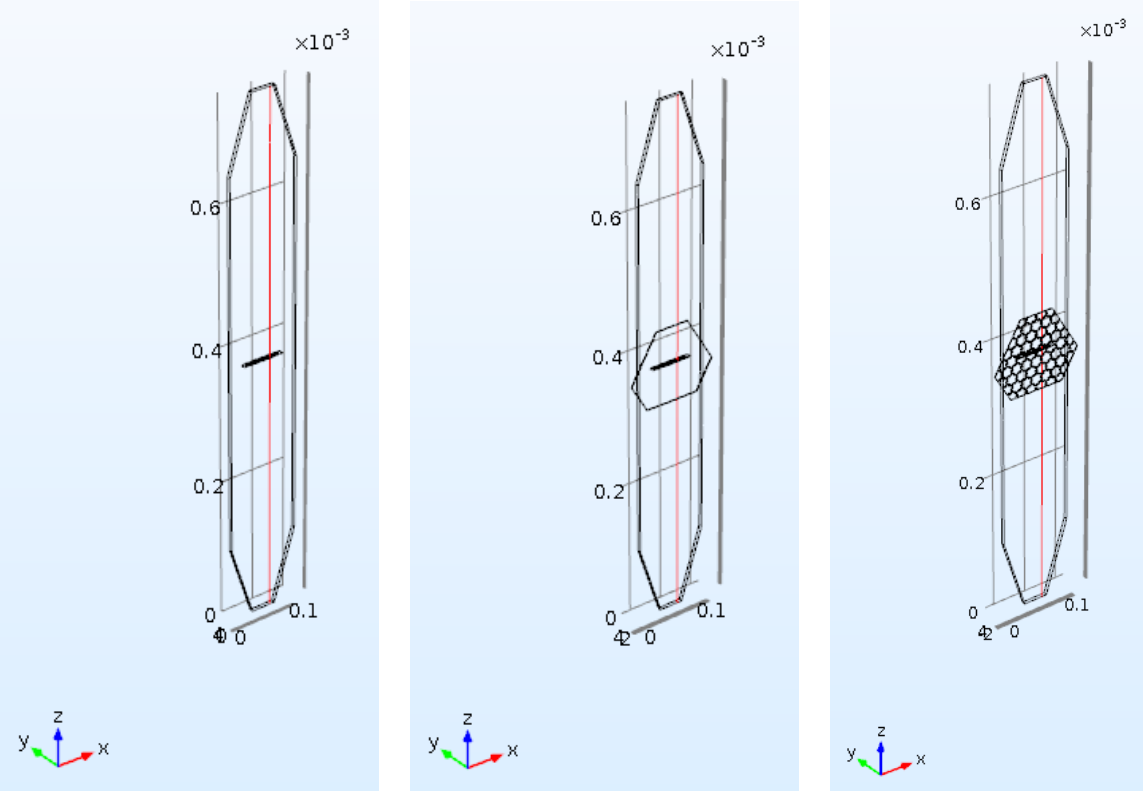

Figure B.6: Geometry back planes

Materials & Meshing

Since only weak fields are being considered, hysteresis effects were disregarded and the steel material of the plate and back plane was modeled linearly with a relative permeability of 225 [27].The other material used in these models is air, with a relative permeability of 1. The model was meshed using free tetrahedral meshing.

Boundary conditions

The physics used in this model is Magnetic Fields, No Currents in COMSOL Multiphysics and the results are conducted for a stationary study. The background magnetic field was set as in table B.1. The Magnetic Flux Conservation was set for the domains of the specimen and the back plane. For the outside boundaries of the air around the specimen the External Magnetic Flux Density boundary condition was used. To reduce computation time there was made use of the symmetry of the geometry for that reason only half of the geometry needed to be modeled. The boundary condition on the symmetry plane that was used is the Zero Magnetic Scalar Potential. This boundary applies since the magnetic field is perpendicular to this plane.

Results

The results obtained from the FEM model are taken along the red line. This line is modeled on top of the plate for the entire length of the plate. Since the back plane is behind the Hall sensors the results are taken in front of the back plane. The results for three different back planes are shown in figures B.7, B.8 and B.9.

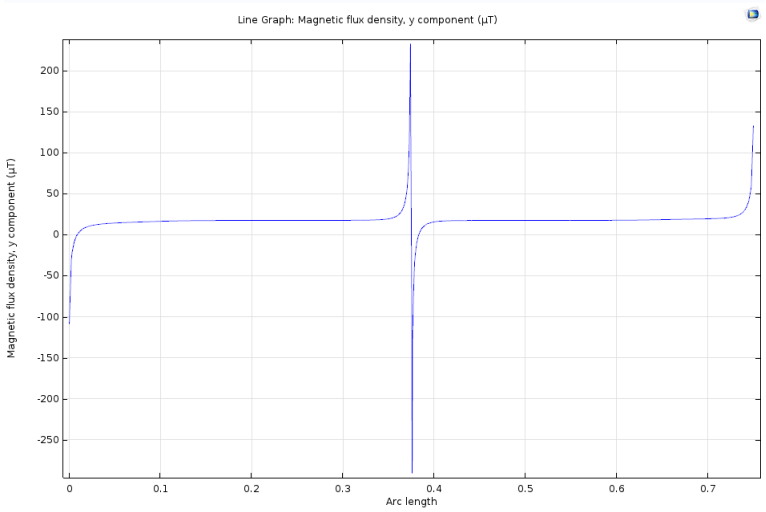

Figure B.7: B_y without a back plane

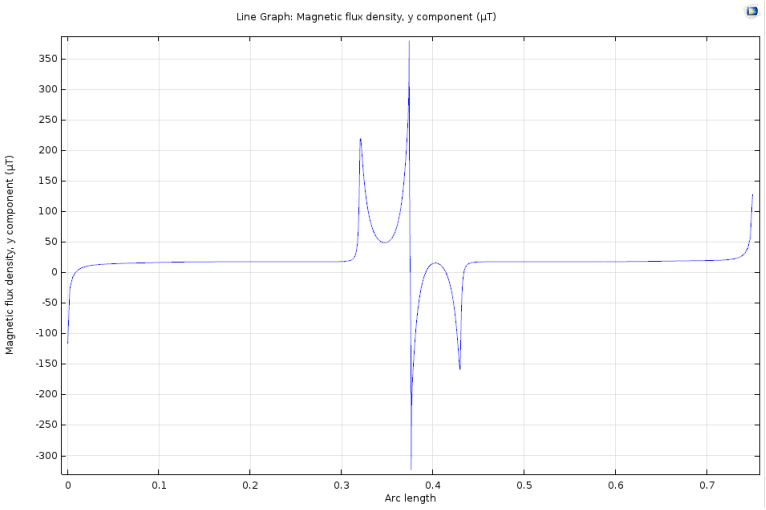

Figure B.8: B_y with a solid back plane

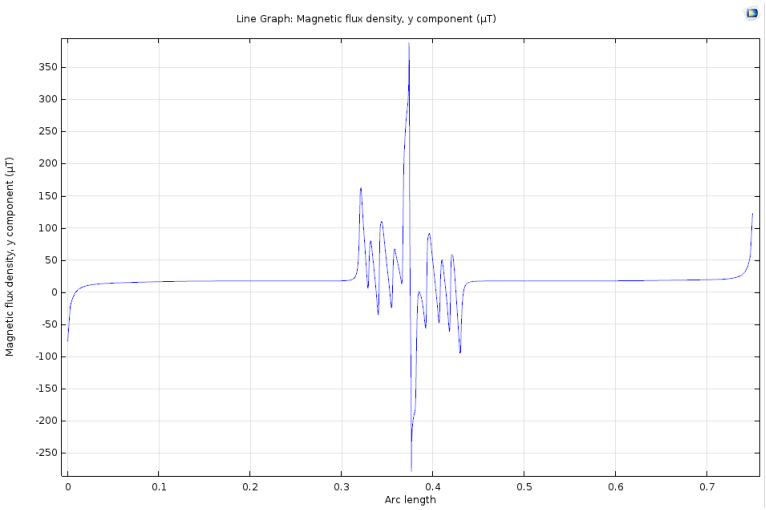

Figure B.9: B_y with the CrackGuard back plane

Bibliography

[1] Courant–friedrichs–lewy condition. https://en.wikipedia.org/wiki/Courant%E2%80%93Friedrichs%E2%80%93Lewy_condition#CITEREFCourantFriedrichsLewy1928. Accessed: 2018-02-04.

[2] Carbon content s235. https://www.azom.com/article.aspx?ArticleID=6022. Accessed: 2018-02-03.

[3] Cover picture. https://www.extremetech.com/wp-content/uploads/2011/09/micro-crack-steel-canyon.jpg. Accessed: 2018-03-20.

[4] Euler forward method. http://mathworld.wolfram.com/EulerForwardMethod.html. Accessed: 2018-02-04.

[5] Hall sensor. http://www.wuntronic.de/en/USB-Tesla-Meter-Gauss-Meter-with-USB.html. Accessed: 2017-11-03.

[6] Magnetic definitions. https://www.britannica.com/science/magnetic-permeability, . Accessed: 2018-03-07.

[7] Magnetic domains. https://www.nde-ed.org/EducationResources/CommunityCollege/MagParticle/Physics/MagneticDomains.html, . Accessed: 2018-02-03.

[8] Fatigue crack initiation. https://www.nde-ed.org/EducationResources/CommunityCollege/Materials/Structure/fatigue.htm. Accessed: 2017-05-24.

[9] Matlab function: smooth. https://nl.mathworks.com/help/curvefit/smooth.html. Accessed: 2018-01-31.

[10] C. Bathias and A. Pineau. *Fatigue of Materials and Structures - Fundamentals*. John Wiley & Sons, 2010.

[11] Matzhanin G. A. Beissner, R. E. and C. M. Teller. Nde applications of magnetic leakage field methods. *SWRI Report*, NTIAC-80-1, 1980.

[12] BS7910:2013. Guide to methods for assessing the acceptability of flaws in metallic structures. Standard, The British Standard Institution, dec 1999.

[13] M. P. Connolly and R. Collins. The measurement and analysis of semi-elliptical surface fatigue crack growth. *Engineering Fracture Mechanics*, 26:897–911, 1987.

[14] D.J. Craik and M. J. Wood. Magnetization changed induced by stress in a constant applied field. *Journal of Physics D: Applied Physics*, 3:1009–1016, 1970.

[15] B. D. Cullity and C. D. Graham. *Introduction to Magnetic Materials*. John Wiley & Sons, 2008.

[16] K.H.J. Buschow & F.R. de Boer. *Physics of Magnetism and Magnetic Materials*. Kluwer Academic/Plenum Publishers, 2003.

[17] A. Dubov. A study of metal properties using the method of magnetic memory. *Metal Science and Heat Treatment*, 39:401–5, 1997.

[18] L. Jiles, D.C.& Li. A new approach to modeling the magnetomechanical effect. *Journal of Applied Physics*, 95(11):7058, 2004.

[19] Thoelke J. B. Jiles, D.C. and M. K. Devine. Numerical determination of hysteresis parameters for the modeling of magnetic properties using the theory of ferromagnetic hysteresis. *IEEE Transactions on Magnetics*, 28(1):27–35, 1992.

[20] I. E. Kopsov. Stress intensity factor solution for a semi-elliptical crack in an arbitrarily distributed stress field. *Int J Fatigue*, 14:399–402, 1992.

[21] J.Zuidema M. Jansen and R.J.H. Wanhill. *Fracture Mechanics*. VSSD, 2002.

[22] A.J. McEvily. Fatigue crack thresholds. *Fatigue and Fracture, ASM Handbook*, 19:134–152, 1996.

[23] H.W.L. Naus. Theoretical developments in magnetomechanics. *IEE Transactions On Magnetics*, 47(9): 2155–2162, 2011.

[24] E. Ramsden. *Hall-Effect Sensors - Theory and Applications*. Elsevier, 2006.

[25] D. Roylance. *Fatigue*. Massachusetts Institute of Technology, Department of Materials Science and Engineering, 2001.

[26] M. P. van der Horst and M. L. Kaminski. Slit induced self magnetic flux leakage in a square steel plate. .

[27] M. P. van der Horst and M. L. Kaminski. Magnetic properties of structural steels for simulation of crack monitoring by finite element method. .

[28] M. P. van der Horst and M. L. Kaminski. Testing and numerical simulation of magnetic fields affected by presence of fatigue cracks. *Proceedings of the Twenty-fourth (2014) International Ocean and Polar Engineering Conference*, 2014.